UNIVERSIDAD CARLOS III DE MADRID
ESCUELA POLITÉCNICA SUPERIOR

DYNAMIC MODELS FOR FLAPPING-WING MICRO-AIR VEHICLES

Bachelor Thesis

Author
Blanca Martínez Gallar

Leganés, June 2015

Department of Aerospace Engineering
ESCUELA POLITÉCNICA SUPERIOR

DYNAMIC MODELS FOR FLAPPING-WING MICRO-AIR VEHICLES

Bachelor in Aerospace Engineering

Author
Blanca Martínez Gallar

Supervisor
Manuel García-Villalba Navaridas

Leganés, June 2015

People, we have perfectly ordinary plumbing.

Steven Vogel

If you want to know the truth of who you are, walk until not a person knows your name. [...] A long stretch of road will teach you more about yourself than a hundred years of quiet introspection.

Patrick Rothfuss

When everything seems to be going against you, remember that the airplane takes off against the wind, not with it.

Henry Ford

Acknowledgements

I will like to express my immense gratitude especially to the person that have make this possible, that have concerned and interest from the beginning, Manolo and Óscar. It has been a pleasure to work with them in the Aerospace Department. It is a big list of thing I have learned during those meetings. I want to give a really really really big thank you to Gonzalo. He was always there to help me and care and, of course, he had to spend way to much time with me, but there were good moments I will remember. For all the things I have learned during these four years, personally and academically, I will like to thank all the Aerospace Engineering Department and all the people from my class. In one way or the other they have contributed to the great experience and the great memories I now carry with me.

Some of the people I have met in this degree have become some of the best people I have ever gotten the pleasure to know. And to them I also want to give a more specific thank you. They have been there in every step of the way, sharing good and bad moments.

However all this great thing could not have been possible without the always caring, always supportive presence of my family. They have helped me and have taken care of me when not everything was going as planned. Their constant comfort has given me way more that I realized at the moment.

Abstract

The project presents the development of a computational integrated model of the flight of a MAV. The created tool is validated and tested for fixed and flapping wing configurations. This preliminary design integrates the computation of the aerodynamic forces of unsteady flow of flapping wings and the dynamic behaviour dependent on those forces. Linear and non-linear aerodynamic estimations are used. The dynamic model is completely originated in the project, as the integration of both parts.

Contents

List of Figures

List of Tables

CHAPTER

ONE

Introduction

1.1 Technological relevance

In this project, the principal aim is to develop a computational integrated model of a Micro-Air Vehicle (MAV) inspired in the flight of insects and small birds. Nowadays there is a great interest in elaborating efficient MAVs. This kind of vehicles has a miniature size and they are able to fly at significant low velocities which raises the problem that the same procedures and theories applied to conventional aircraft of larger dimensions cannot be applied. The interest in this kind of devices is due to the great range of different missions where they can be employed. For example, MAVs can be used as an identification mechanism for searching and rescuing activities as well as exploration of areas of difficult access; especially in conditions of fire, a nuclear accident, etc.

As birds and insects are the true masters on this field, it is only natural that these projects propose the computational study of the flight of a simplified MAV model that resembles the shape of an insect. Recent advances have permitted the improvement of MAVs. One of the most clear and remarkable example is the hummingbird created by Aerovironment [1]. However, the area of improvement for these machines is still very broad. In particular, the artificial hummingbird is controlled by remote control as the payload is extremely limited. In addition, one of the greatest limitations of these vehicles is that they only work properly at their design conditions. When these conditions are not the ones met, their characteristics and performance deteriorate notably. This is one of the reasons why it is so necessary to have a deeper understanding of the physics behind the flight of insects and small birds.

In this project the geometry of the MAV will only include the body or fuselage and the wings, for simplicity. In order to ensure rotational stability, a tail is going to be incorporated to the geometry. The flight dynamics of an insect covers three differentiated aspects that need to be taken into account together. These aspects are the kinematics of the motion of the wings, the computation of the aerodynamic forces resulting from the motion of these wings in the air and, finally, the movement of the insect as a result of those aerodynamic forces together with the gravity force. The kinematics of the wings includes an up-down motion and lateral rotations and oscillations. This will result in large changes of the angle of attack with respect to the wing surface. This aspect in this project will be imposed externally with

a simplified motion as it is a preliminary design. In posterior studies this motion may evolve to an imitation of the actual behaviour of insects during flight. The calculation of the forces is going to be solved with an unsteady panel method using potential theory. Once the aerodynamic forces are estimated, the motion of the MAV is performed through the resolution of the equations of a rigid body motion for the body of the insect. The two systems of equations are coupled and so they need to be worked out together as the motion of the body will affect the flow of air around the MAV and vice versa.

1.2 State of the art

The study of the physics for the efficient development of MAVs has become of great interest worldwide during this last decade. Recently, a book has been published about the aerodynamics of flapping wings [2] where the current knowledge about this topic is summarized. According to Elsevier journals, the most cited article since 2010 in Aerospace Sciences is a review on the subject of flapping wings [3]. In 2012, Orlowski [4] centered in one review, all the main advances done in the last decades in this field of study.

The efficient design of MAVs is a great challenge as the variables involved in the design are numerous such as the geometry of the wings and fuselage, the control surfaces, the properties of the materials, the kinematics of the wing or the flight conditions. Flapping wings have an outstanding advantage compared to regular aircraft fixed wings. As said in [5], a fixed wing only produces lift and so it must have an external source of thrust. However, birds and insects use flapping wings as a way to generate both, lift and thrust. This philosophy is somehow similar in helicopters where the rotors also produce lift and thrust.

The aerodynamic model used to estimate the forces generated by the wings is also of great importance for the design of a MAV. Quasy-steady models appear insufficient to account for the mean lift recorded in the cases available [6]. This is why other methods have been applied, one of the most important methods is computational fluid dynamics (CFD). It may not be as simple as the previous one, but recent advances in technology and computational methods have made this area more tempting for research. Inside the CFD area there are many different methods of computation. In fact in [7], an improved method for incompressible viscous flows around rigid particles is presented. This kind of simulations can be performed in two or three dimensions.

Another variable studied is the distribution of the mass along the MAV. For simplicity, many models assume that all the mass is concentrated on the fuselage, so the wings are mass-less and the body can be interpreted as a rigid body. In [8] a review of the main advances done in the last decades is presented. One of the models described studies the motion of an ornithopter with five bodies to take into account the body, wings and tail of the vehicle as shown in figure 1.1.

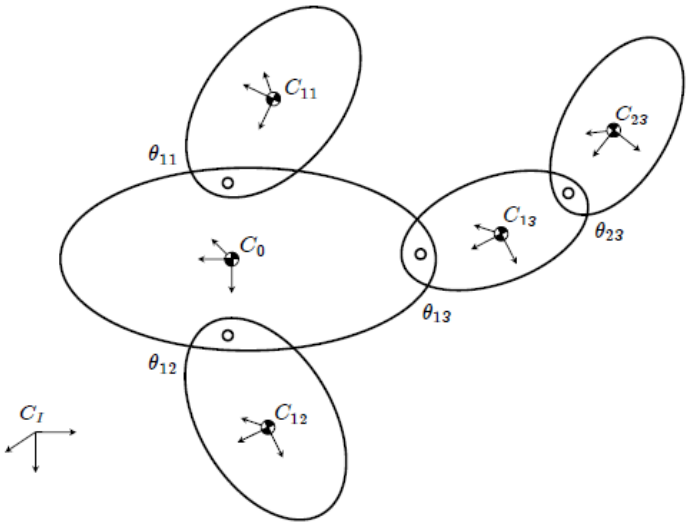

Figure 1.1: Layout of the multibody configuration of an ornithopter

The stability of the body is crucial in order to be able to fly. This stability, as in regular aircraft, can be achieved by means of including aerodynamic control surfaces for example a horizontal or a vertical tail. However there are other methods that can be used such as the one explained in [9]. The main idea behind this way to control the pitching rotation is the change of the position of the center of mass. In order to do so, the body is divided in two parts: thorax and abdomen. They are linked and can rotate with respect to each other. The forward and aft movement of the abdomen changes the position of the center of gravity. This is the actual mechanism used by butterflies.

Recently in Delft University of Technology, they had built a Flapping Wing Micro Air Vehicle (FWMAV), the *DelFly*, that can be electronically controlled by a person from the ground. This allows to have actual experimental data of this kind of devices in order to compare them to the results obtained by different models performed as explained in [10]. This robot, for example, has horizontal and vertical tails to stabilize it. Another university that has built one FWMAV is Harvard University. Its *RoboBee* uses a modular approach to flight control [11].

Nowadays there is a lot of controversy regarding the topic of MAVs. There has been several encounters of this aerial vehicles with commercial airliners [12]. This has lead to the necessity of establishing some regulations in order to avoid this kind of accidents to happen again. The Federal Aviation Authorities (FAA), together with Law Enforcement Agencies (LEAs), have started to address these activities and starting to implement several regulations [13].However the aim of this project is to create a computational tool, not a physical object and so the MAV regulations do not apply to this project.

1.3 Objectives

The main objective of this project is to develop a computational integrated model of the flight of a MAV. It is a preliminary study to integrate non stationary aerodynamics of flapping wings with the orientation and trajectory of the body. Some inputs for the model are going to be imposed such as the geometry of the MAV, the mass of the body, the initial conditions of the flight and the movement of the wings with respect to the body of the MAV.

Once the inputs have been specified, the computational model will provide the value of the resulting forces as well as the trajectory followed by the MAV. This outputs will be calculated by means of two different parts, one is the aerodynamic estimations and the second one is the dynamic model itself.

The aerodynamic code used in this project is taken from other sources. The part that is fully implemented and validated in this project is the dynamic model. This simplified model will be tested in different cases.

At the end of this project, it is expected to acquire a computational tool that will be useful in order to help future optimum and robust design of MAVs.

In order to study the correct integration of the tool, the simulations will focus on the longitudinal motion with symmetric flight.

CHAPTER

TWO

Methodology

2.1 General view

The dynamic behaviour of a body is related to the forces and moments applied to it. These forces and moments can be generated due to numerous reasons. In aircraft dynamics, the most common ones are the aerodynamic forces (including thrust) on the one side, and the weight ($W = mg$) on the other side.

Wings are the main foundation of the aerodynamic forces. The forces generated by the wings can be decomposed in the body reference frame, giving as a result an upward force that is called lift (L) and also a force in the horizontal direction that, depending on its sign, is defined as thrust (T) or drag (D). If the movement of the wings with respect to the body is non symmetrical, then, lateral forces will also appear.

The drag force is produced due to several effects, such as the friction of the fluid with the body (*parasite drag*), the drag caused by lift (*induced drag*), the drag influenced by the wake the body leaves in the fluid (*wake drag*), etc.

This variety of forces will create moments on the aircraft as they are not all applied at the center of mass. From these forces, the most difficult ones to assess are the aerodynamic forces. For conventional fixed wings, as the ones found in aircraft, the estimation of these forces has been extensively studied and there are different ways to compute it to determined levels of accuracy. However, in the case of flapping wings, this field is still in research and unknown to some extent. They are not easily computed. The way to proceed will be better detailed in section 2.4.

In order to see how the forces and moments affect the movement of the body, Newton's Second Law of Motion that relates the forces with the accelerations of the body is applied. Forces ($\mathbf{F}$) are linked to linear momentum ($m\mathbf{v}$, where m is the mass of the body and $\mathbf{v}$ is the linear velocity vector) while moments ($\mathbf{M}$) are linked to angular momentum ($\mathbf{H} = I\boldsymbol{\omega}$, I is the inertia tensor and $\boldsymbol{\omega}$ is the angular velocity vector). They are defined as follows:

$$\sum \mathbf{F} = m\frac{d\mathbf{v}}{dt} \tag{2.1}$$

$$\sum \mathbf{M} = \frac{d\mathbf{H}}{dt} \tag{2.2}$$

If the forces are known, then the accelerations ($\frac{d\mathbf{v}}{dt}$) can be easily found. Once the accelerations are computed, there is an integration process that needs to be carried out to calculate the velocity and therefore, the position of the body too. The integration is done employing numerical schemes that will be explained in section 2.3.

The equations can be solved in any reference frame. However, the resolution in some axes is easier that in others. For our purpose, it would be advantageous to express everything in an inertial reference frame to have a global view of the entire movement. However, the moment equation is quite arduous in such reference frame and so body axes are going to be used. Nevertheless, the linear motion and the forces are going to be solved with respect to an inertial reference frame.

2.1.1 Reference frames

Several reference frames are going to be used during the extent of this project. They are explained below:

- **Inertial reference frame**
  This frame is fixed to a certain position so it will not move or change over time. It is needed in order to have a sense of what the position of the body is with respect to its original location. These axes could have any orientation, but it is chosen to have its origin as the body reference frame at the initial configuration. The orientation of these axes will determine the orientation of Earth (*"the ground"*) in the simulation.

- **Body reference frame**
  As its own name reveals, this reference frame is fixed to the body. The axes are set in a particular way in the directions of the body. For instance, the X direction refers to the longitudinal axis. The sense of the vector is oriented to the rear part of the body. The Z axis points upwards, approximately being a normal vector to the surface of the wing. The origin of this reference frame is the center of gravity (CG). In figure 2.1 both axes, inertial and body, can be seen.

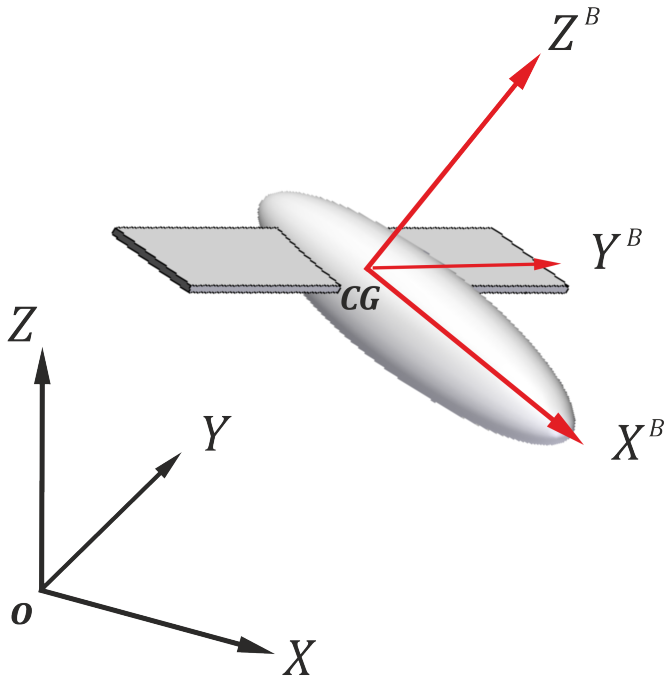

Figure 2.1: Inertial (X, Y, Z) and body (X^B, Y^B, Z^B) reference frames

- **Wing reference frame**
  The wing axes follow the same direction as the body axes. The wing reference frame has its origin located at the point where the aerodynamic forces are calculated, the center of pressure of the wing (CP). This point is located at a quarter chord distance of the leading edge of the wing and the other two position components are zero. However this reference frame is fixed with respect to the body, and so it does not account for the movement of the wing with respect to the body when there is a flapping motion.

  When the wing is not fixed to the body, it will have a prescribed motion where two kinds of movement (heaving and pitching) can be imposed. This motion is defined according to several variables explained more deeply in section 2.4. It is given with respect to the wing reference frame. The change from the wing reference frame to the actual fixed axes to the wing is given directly by the aerodynamic code and the resultant forces are given expressed in wing axes. It can be seen in figure 2.2, the difference between the body axes (X^B, Y^B, Z^B), wing axes (X^W, Y^W, Z^W) and the wing fixed axes (X^{WF}, Y^{WF}, Z^{WF}).

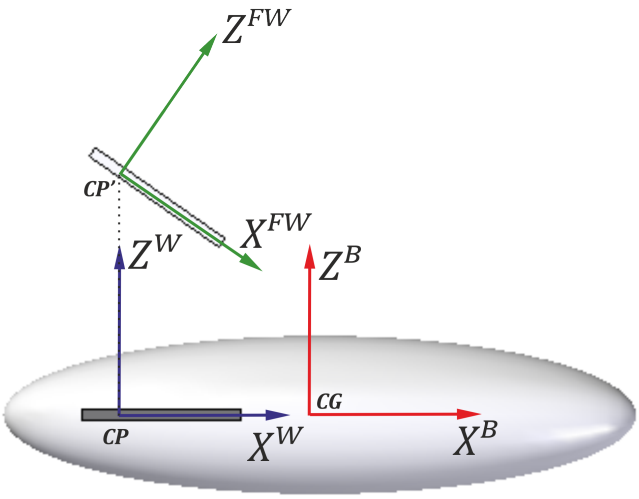

Figure 2.2: Body (X^B, Y^B, Z^B), wing (X^W, Y^W, Z^W) and the wing fixed (X^{WF}, Y^{WF}, Z^{WF}) reference frames

- **Flight mechanics reference frame**
  The flight mechanics reference frame is used in some validation cases of this project, therefore it is included in this section. This reference frame is the body reference frame usually used in flight mechanics problems instead of the aerodynamic axes used in the body reference frame of this project. The origin of both reference frames is the same, as well as the Y direction. However the X direction points upstream and the Z direction is oriented downwards so: $X^{FM} = -X^B$ and $Z^{FM} = -Z^B$, as it can be seen comparing the reference frames in figure 2.3.

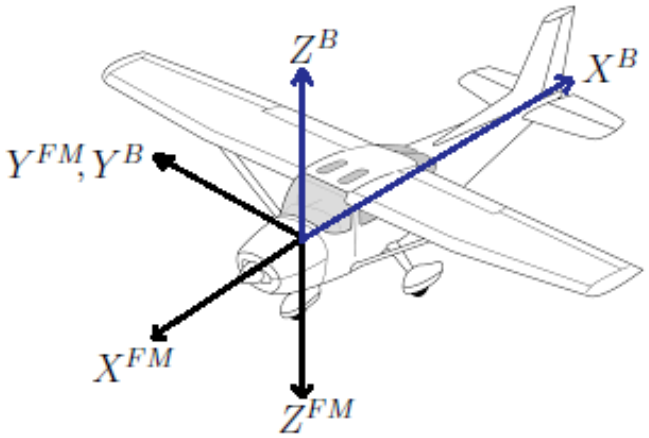

Figure 2.3: Body (X^B, Y^B, Z^B) and flight mechanics (X^{FM}, Y^{FM}, Z^{FM}) reference frames

- **Euler angles**
  Even if the orientation of the body will be defined by the quaternions explained in section 2.2, at the beginning of the motion ($t = 0\ s$) the inertial and the body references frame are located at the same origin. Hence the initial positions of the center of gravity with respect to the inertial reference frame are:

$$x_0 = 0\ m \qquad y_0 = 0\ m \qquad z_0 = 0\ m$$

  Nevertheless, the orientation of the body and the inertial axes do not have to coincide. In order to set this initial deviation of the body reference frame with respect to the inertial reference frame, the Euler angles (ϕ_0, θ_0, ψ_0) are going to be used. They are determined as shown in figure 2.4.

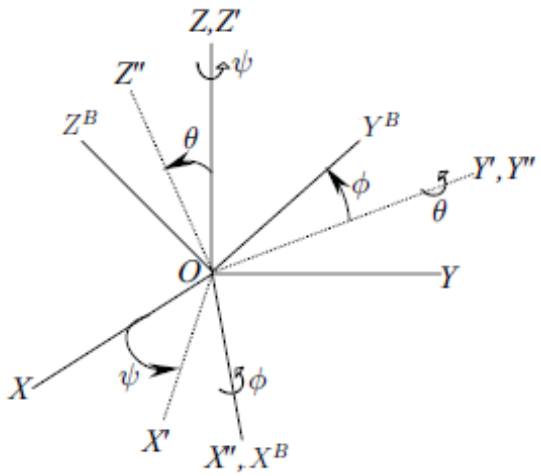

Figure 2.4: The Euler angle orientation, $(\psi)_3$, $(\theta)_2$, $(\phi)_1$.Adapted from [14]

The angles ϕ, θ and ψ are the rotations around the X, Y and Z axis respectively. The first rotation is performed of an angle ψ along Z axis of the inertial reference frame. The Y rotation of angle θ is done with respect to Y'. And in order to rotate an angle of ϕ is needed X" axis. After all of this is carried out, the body reference frame has been reached.

2.1.2 Moments in body axes

Let us now see the reason why body axes are far more convenient in order to compute the moments. For equation 2.2, it is known that a moment is defined as the time derivative of the angular momentum (**H**), which contains the moments and products of inertia of the inertial tensor (I) with respect to the reference frame chosen. If those axis are fixed to the body, the moments of inertia will remain constant instead of changing over time as the body changes with respect to an inertia reference frame.

From the Coriolis theorem, it is known that the time derivative employing body reference frame (X^B, Y^B, Z^B) should be as follows:

$$\frac{d\mathbf{H}}{dt} = \left[\frac{d\mathbf{H}}{dt}\right]_B + \boldsymbol{\omega} \times \mathbf{H} = I\boldsymbol{\alpha} + \boldsymbol{\omega} \times (I\boldsymbol{\omega}) \tag{2.3}$$

where $\boldsymbol{\omega} = p, q, r$ is the angular velocity in body axes, $\boldsymbol{\alpha} = \dot{p}, \dot{q}, \dot{r}$ is the angular acceleration in body axes and I is the inertia tensor that is defined as:

$$\mathsf{I} = \begin{pmatrix} I_x & I_{xy} & I_{xz} \\ I_{yx} & I_y & I_{yz} \\ I_{zx} & I_{zy} & I_z \end{pmatrix} \tag{2.4}$$

We are assuming that our bodies are symmetric with respect to the plane $X^B Z^B$ and so: $I_{xy} = I_{yz} = 0$. That leaves only four variables of the inertia tensor: I_x, I_y, I_z and I_{xz}. So at the end, the resulting equations for the moments in body axes are:

$$L = I_x\dot{p} - I_{xz}(\dot{r} + pq) - (I_y - I_z)qr \tag{2.5}$$
$$M = I_y\dot{q} - I_{xz}(r^2 - p^2) - (I_z - I_x)rp \tag{2.6}$$
$$N = I_x\dot{r} - I_{xz}(\dot{p} - qr) - (I_x - I_y)pq \tag{2.7}$$

2.2 Orientation of the body (quaternions)

In order to track the orientation of the body during the evolution of the movement with time, several possibilities are available. Due to the singularities that can be found when implementing the regular Euler angle rotations to the body, it was decided to represent those rotations in a different manner. The quaternion, a representation composed of four variables, was chosen. The quaternion, as explained by Tewari [14], is based upon the Euler-axis/principle angle combination. So the four variables that compose the quaternion represent the direction of the axis of rotation and the magnitude of the angle that the vector is rotated around the direction previously defined by the quaternion. The axis of rotation is described as: $\vec{e}(t) = e_x\vec{i} + e_y\vec{j} + e_z\vec{k}$ and the angle is defined as φ. So the quaternion is defined

by four dependent scalar parameters Q_1, Q_2, Q_3 and Q_4. The first three parameters form the *vector part* of the quaternion,

$$\mathbf{Q} = \{Q_1, Q_2, Q_3\} \tag{2.8}$$

and the fourth one represent the *scalar part*. From the definition of the quaternion is can be said that:

$$Q_1 = e_x \sin(\varphi/2) \tag{2.9}$$
$$Q_2 = e_y \sin(\varphi/2) \tag{2.10}$$
$$Q_3 = e_z \sin(\varphi/2) \tag{2.11}$$
$$Q_4 = \cos(\varphi/2) \tag{2.12}$$

In order to compute the way the quaternion changes with time, its time derivative is needed. In this study, the equation used is the one already described in [14] and it is the following:

$$\frac{d\{(\mathbf{Q}, Q_4)\}^T}{dt} = \frac{1}{2}\Omega\{\mathbf{Q}(t), Q_4(t)\}^T \tag{2.13}$$

where Ω is a skew-symmetric matrix that depends on the angular velocity components in body axis ($\vec{\omega} = \{p, q, r\}$):

$$\Omega = \begin{pmatrix} 0 & r & -q & p \\ -r & 0 & p & q \\ q & -p & 0 & r \\ -p & -q & -r & 0 \end{pmatrix} \tag{2.14}$$

Therefore the quaternion will give information of how the body is rotating. With this information, the rotational matrix (R) that allows the change from inertial axis to body axis can be computed:

$$R = ({Q_4}^2\mathbf{Q}^T\mathbf{Q})\mathbf{I} + 2\mathbf{Q}\mathbf{Q}^T 2Q_4 S(\mathbf{Q}) \tag{2.15}$$

where $S(\mathbf{Q})$ is the following matrix:

$$\mathsf{S}(\mathbf{Q}) = \begin{pmatrix} 0 & -Q_3 & Q_2 \\ Q_3 & 0 & -Q_1 \\ -Q_2 & Q_1 & 0 \end{pmatrix} \tag{2.16}$$

It is important to keep in mind that the quaternion must be a unitary vector:

$$Q_1^2 + Q_2^2 + Q_3^2 + Q_4^2 = 1 \tag{2.17}$$

In order to calculate the initial quaternion for the body, one of the options is to compute first the rotational matrix and from it, the information is extracted to solve the initial quaternion. The rotational matrix is computed with the Euler angles (see figure 2.4) where each angle corresponds to a rotation in one of the axis X (*axis 1*), Y (*axis 2*) or Z (*axis 3*) as follows:

$$R = R_1(\phi)R_2(\theta)R_3(\psi) = \\ = \begin{pmatrix} \cos\theta\cos\psi & \cos\theta\sin\psi & -\sin\theta \\ (\sin\phi\sin\theta\cos\psi - \cos\phi\sin\psi) & (\sin\phi\sin\theta\sin\psi + \cos\phi\cos\psi) & \sin\phi\cos\theta \\ (\cos\phi\sin\theta\cos\psi + \sin\phi\sin\psi) & (\cos\phi\sin\theta\sin\psi - \sin\phi\cos\psi) & \cos\phi\cos\theta \end{pmatrix} \tag{2.18}$$

The direction ($\mathbf{e}$) of axis of rotation of the quaternion is defined as the eigenvector corresponding to the eigenvalue equal to 1 of the rotational matrix. And the angle of rotation (φ) is the imaginary part of the complex pair of eigenvalues that correspond to the other eigenvalues of that matrix. So the quaternion can be calculated from equations 2.9, 2.10, 2.11 and 2.12.

2.3 Numerical Schemes

A numerical scheme needs to be used as a mean to compute the evolution of the body. The derivatives of the variables are computed and then the numerical scheme makes possible the integration to estimate the values of the variables at the following time step.

There are a multitude of different schemes that could be used. The higher the order of the method, the more accurate the results, in principle. The method that was carried out was an Adam Bashforth scheme. This was decided due to the desire of combining an aerodynamic code explained in section 2.4 with the dynamic model. As this code did not provide the value of the forces at intermediate fractions of a time step, no multi-stage methods could be applied such as Runge Kutta.

A second order Adam Bashforth method is the one applied in this analysis. This means that there is a necessity for information for the previous two time steps, as it is a linear multi-step method. It is interesting to notice that the method is explicit, and so the difficulty of expressing the derivatives of the variables as a function of known variables is reduced considerably. The definition is the next one:

$$u^{n+2} = u^{n+1} + \frac{\Delta t}{2}[-f(u^n) + 3f(u^{n+1})] \tag{2.19}$$

As this numerical scheme needs information from the previous two time steps, in order to calculate the values of the variables for the second time step, a first order Adam Bashforth, also known as the Euler method, is applied:

$$u^{n+1} = u^n + \Delta t f(u^n) \tag{2.20}$$

2.4 Aerodynamic Computations

The aerodynamic forces that are generated due to the motion of the body studied need to be estimated. In order to do so, two different approaches are used. One consist on applying linearized aerodynamic forces coming from the stability derivatives of the aircraft, while the other compute directly the forces by a panel method taking into account unsteady effects.

2.4.1 Linearized aerodynamic forces (*Option 1*)

This approach is going to be used during the validation of the dynamic model and also as a tool for the results. The linearization of the aerodynamic forces is introduced when applying small-disturbance notation to equations 2.1 and 2.2. The complete equations can be found in [15].

The main idea is that the forces and moments part from reference values (X_0, Y_0, Z_0, L_0, M_0, N_0) and that according to the evolution of the variables of the system, the values of these forces and moments will change linearly with those variations. The typical reference condition chosen is steady level flight ($Lift = weight$) at equilibrium ($\mathbf{M} = \{L, M, N\} = \{0, 0, 0\}$). Expressing these conditions in flight mechanics reference frame leads to:

$$X_0 = mg \sin\theta_0 \tag{2.21}$$
$$Y_0 = 0 \tag{2.22}$$
$$Z_0 = -mg \cos\theta_0 \tag{2.23}$$
$$L_0 = M_0 = N_0 = 0 \tag{2.24}$$

Depending on the variation of the variables of the system, the forces and moments are going to change. The variables of the system are:

- Position of the CG in inertial axis: (x, y, z)
- Linear velocity of the CG in inertial axis: (u^I, v^I, w^I)
- Angular velocity in body axes: (p, q, r)

The longitudinal variables are u, w and q. While the lateral variables are v, p and r. Linear aerodynamic theory is used to obtain the following variations of the forces and moments:

$$\Delta X = X_u \Delta u + X_w w + X_{\dot{w}} \dot{w} + X_q q \tag{2.25}$$
$$\Delta Y = Y_v v + Y_p p + Y_r r \tag{2.26}$$
$$\Delta Z = Z_u \Delta u + Z_w w + Z_{\dot{w}} \dot{w} + Z_q q \tag{2.27}$$
$$\Delta L = L_v v + L_p p + L_r r \tag{2.28}$$
$$\Delta M = M_u \Delta u + M_w w + M_{\dot{w}} \dot{w} + M_q q \tag{2.29}$$
$$\Delta N = N_v v + N_p p + N_r r \tag{2.30}$$

where $X_{u,w,\dot{w},q}$, $Y_{v,p,r}$, $Z_{u,w,\dot{w},q}$, $L_{v,p,r}$, $M_{u,w,\dot{w},q}$ and $N_{v,p,r}$ are the stability derivatives of the system.

Notice that the actuation of the control surfaces is not taken into account as no kind of control loop is going to be performed. It can be seen in the equations above that the longitudinal forces (X and Z) and the pitching moment (M) only depend on the longitudinal variables. This is due to the fact that a longitudinal motion is perfectly symmetrical hence all the lateral variables are not excited.

On the other hand, the lateral force (Y) and the roll and yaw moments (L and N) only depend on the lateral variables (v, p and r). The assumption that the lateral forces only depend on the lateral variables is not as accurate as in the longitudinal case because the longitudinal variables are going to be excited in a lateral motion. This is due to the fact that the plane of symmetry of the aircraft will no longer be positioned parallel to the plane OX^IZ^I. However, as a first approximation, this effect can be neglected.

Two sets of stability derivatives have been used in this project. The first set corresponds to an aircraft called Lockheed Jetstar, and these coefficients are taken from [16]. In order to be informed about these values, please refer to appendix A.

For the second set of stability derivatives, a program called XFLR5 is used. XFLR5 is an analysis tool for airfoils, wings and planes operating at low Reynolds Numbers [17]. It includes XFoil's Direct and Inverse analysis capabilities and wing design and analysis capabilities based on the Lifting Line Theory, on Vortex Lattice Method, and on 3D Panel Methods. In this project the inviscid 3D Panel Method is used.

This program allows to create the desired wing and tail configuration apart from giving the option to allocate mass inside the structure and also point masses as desired. With this information, this program is capable to provide the moments of inertia and the position of the center of gravity of the created device. Setting a free stream velocity, the stability derivative coefficients can be computed.

The study started out from a model already done and proved stable in [18]. Some changes were performed such as the removal of taper, sweep or dihedral effects because a rectangular wing was desired. Since the aim of this project is to study solely the longitudinal behavior of the drone, there is no need of a vertical tail to provide lateral stability. The body that has been used in this project has the following characteristics, also seen in figure 2.5:

Wing span	$b = 3.28\ m$	Wing mean chord	$c = 0.2\ m$
Tail span	$b_t = 0.7\ m$	Tail mean chord	$c_t = 0.1\ m$
Surface of the wing	$S = 0.656\ m^2$	Surface of the tail	$S_t = 0.07\ m^2$
Wing aspect ratio	$AR_w = 16.4$	Tail aspect ratio	$Ar_t = 7$
Mass of the body	$m = 2\ kg$	Estimated position of CP (wing) or CP' (tail)	$c/4$ or $c_t/4$
Distance from CG to CP'	$d_t = 1.033\ m$	Distance from CG to CP	$d_w = 0.008\ m$
Angle of installation of the wing	$\alpha_{w_I} = 0°$	Angle of installation of the tail	α_{t_I} = -1°
Chord-wise umber of panels	$n_x = 11$	Span-wise umber of panels	$n_y = 66$

Table 2.1: Geometric characteristics of the drone created in XFLR5

Both surfaces, wing and tail, have an airfoil shape of a NACA 0012. It is a symmetric airfoil, therefore at an angle of attack zero gives a lift force and a pitching moment equal to zero. The resulting data acquired from XFLR5 can be found in appendix C.

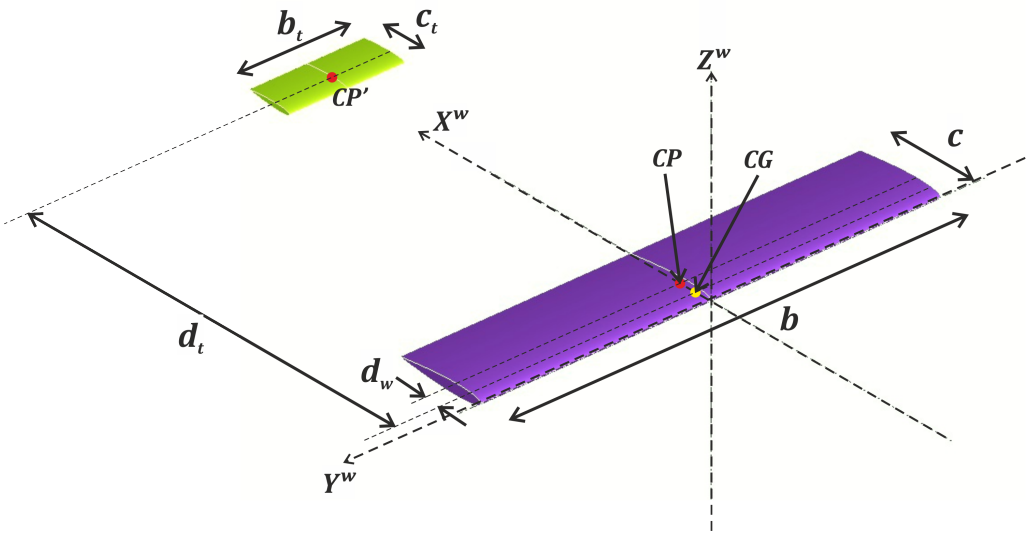

Figure 2.5: 3D view of the wing and tail configuration made in XFLR5

2.4.2 Aerodynamic forces from unsteady panel method (*Option 2*)

A code implemented in [19] has been used to obtain the results of this project. It consists on a potential unsteady aerodynamic model for one or two wings with prescribed motion. This aerodynamic model computes the forces using vortex rings attached to the wing and the wake, dividing them in several panels along the camber line. This method allows to account for unsteady effects.

It allows to compute the lift and the induced drag created by the wing. The wing used is a rectangular wing with no camber and no twist. In order to be able to determine the flapping motion, the following parameters need to be determined.

The heaving and pitching frequency (ω) are defined by a reduced frequency ($k = \frac{\omega c}{U_\infty}$), where c is the chord of the wing and U_∞ is the free stream velocity. The amplitudes of the rotations are defined as h_0 for heaving and Θ_0 for pitching. The mean pitching angle is Θ_M.And the phase shift between both motions is referred as the angle Φ.

There are also other parameters that are used to define the configuration of the wing. To begin with, there is a need to decide the number of panels in the chord-wise and span-wise directions. As the span is larger that the chord, there will be more panels along the Y direction (*spanwise*). The values for these parameters have been set in accordance with [19], yielding a compromise between accuracy and computational time. They are kept constant through all the analysis and equal to:

$$n_x = 4 \qquad\qquad n_y = 20$$

To continue, the number of panels that is going to be selected for the wake along the X direction must be dependent on the velocity and the time step chosen, arriving to the following expression:

$$w_i = \frac{n_c c}{U_\infty \Delta t} \tag{2.31}$$

Obviously, this number needs to be rounded to give an exact amount of panels. Then the width of the wake (defined by w_i) is proportional to a width determined by the chord (c) and the number of chords (n_c) that is desired. The usual range of this number is $n_c = [4, 5]$. The w_i is also inversely proportional to the free stream velocity (U_∞) and the time step size (Δt). The time step size for this method is restricted due to the fact that the maximum desired distance traveled by the body in one time step should not be superior to a quarter chord.

The panels of the wake are shed as the wing moves to at $t = 0$ there is not wake. This affects the calculations of the forces at the beginning of the computations. In order to avoid this problem when using this code for this project, the wake information from a simulation where the wing moves at constant velocity, equal to the free stream selected in the *DyMoFlaps* simulation (see section sec:FinalCode), is loaded to the program and so the first calculations are smoother than if no wake was imposed.

The last thing that is worth mentioning is that the corners of the wing are set according to the wing fixed reference frame. The wing is positioned in a way that the Y axis of the wing fixed reference frame is placed at the location where it is desired that the wing rotates along. For all our cases, this rotation axis is placed at a quarter chord distance from the leading edge.

2.5 Final code implemented (*DyMoFlaps*)

The code that has been developed in this project is a tool put in service to follow the dynamic and kinematic behaviour of a rigid body. This tool has been integrated together with an aerodynamic code explained in 2.4 that allows estimating the forces generated by flapping wings. The final tool has been named *DyMoFlaps* (**Dy**namic **Mo**del for **Flap**ping wing**s**).

In this section the objective is to summarize the steps that are followed by the code in order to determine the motion of the body. In figure 2.6 a flow chart is shown where the main tasks performed are displayed.

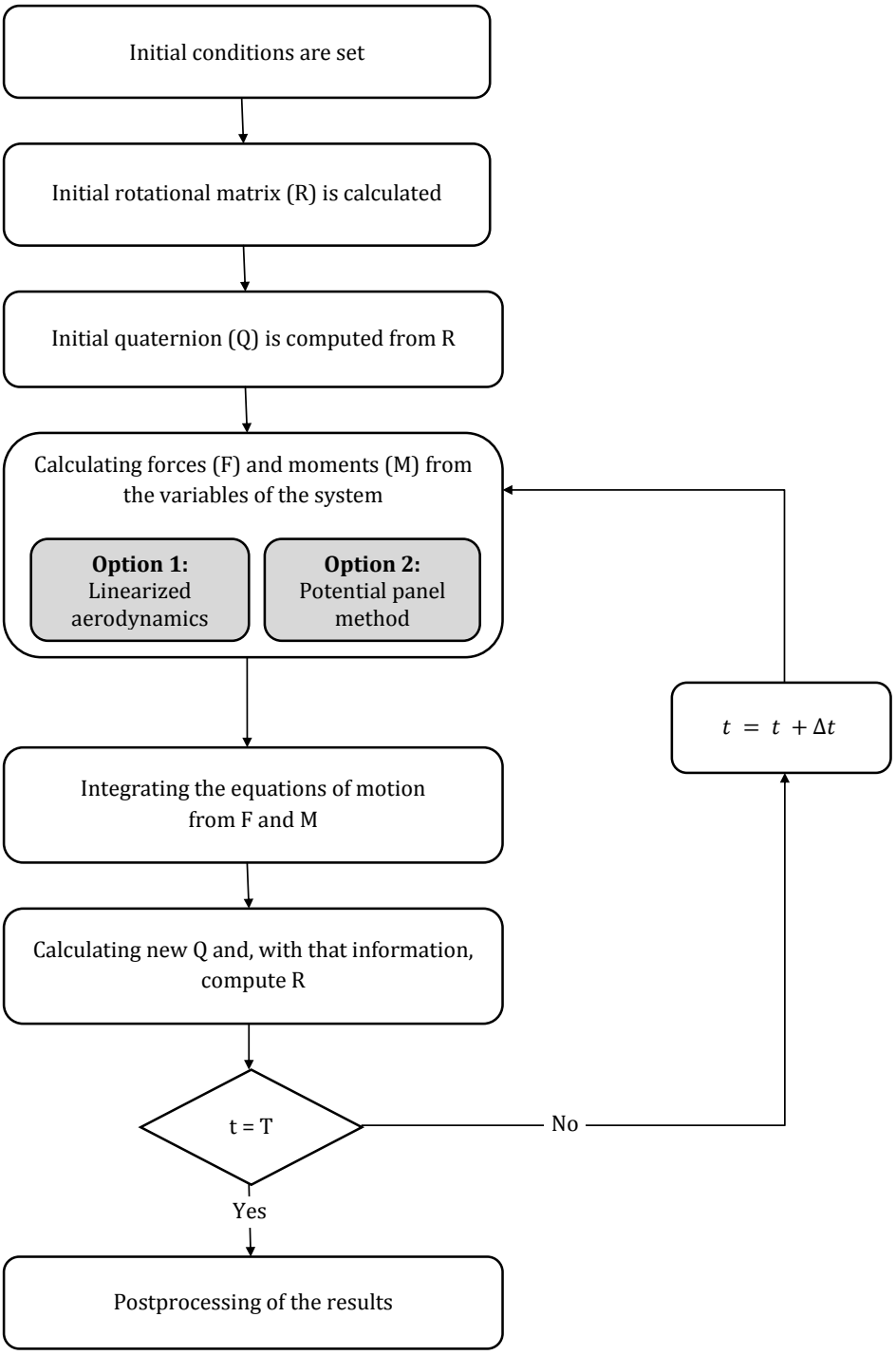

Figure 2.6: Sequence of action followed by *DyMoFlaps*

1. **Data and initial conditions:** Several characteristic magnitudes must be defined. This set of values includes: geometry of the body (c, b, c_t, b_t, d_w, d_t, α_{t_I}), mass and inertia of the body in body axis (m, I_x, I_y, I_z, I_{xz}), constants (gravity acceleration g, density of air at sea level ρ_0), parameters for the aerodynamic code (depending on which one is chosen, see section 2.4) and the time magnitudes (time step size t and final time T). The initial conditions are composed of the position vector (x_0, y_0, z_0), Euler angles (ϕ_0, θ_0, ψ_0), linear velocities with respect to the inertial reference frame (u_0^I, v_0^I, w_0^I) and angular velocities expressed in body axes (p_0, q_0, r_0).

2. **Quaternion set up:** In order to compute the quaternion for the first time step, the rotational matrix is calculated using the Euler angles (ϕ_0, θ_0, ψ_0). Once it is computed, the eigenvalues and eigenvectors are determined and from them the quaternion is defined as in section 2.2.

3. **Forces and moments:** For more information about this task, please refer to section 2.4.

4. **Derivatives of the variables:** All the variables are put into a single vector ($\mathbf{U}$) as follows:

$$\mathbf{U} = [x, y, z, u, v, w, p, q, r, Q_1, Q_2, Q_3, Q_4] \tag{2.32}$$

Coming from Newton's Second Law expressed in equations 2.1 and 2.2, the expressions of the derivatives are the following:

$$\frac{dp}{dt} = \frac{1}{I'_x}L + I'_{xz}N + I'_{xz}(I_x - I_y + I_z)pq - \left[\frac{I_z - I_y}{I'_x} + I_{xz}I'_{xz}\right]qr \tag{2.33}$$

$$\frac{dq}{dt} = \frac{M - pr(I_x - I_z) - I_{xz}(p^2 - r^2)}{I_y} \tag{2.34}$$

$$\frac{dr}{dt} = \frac{1}{I'_z}N + I'_{xz}L - I'_{xz}(I_x - I_y + I_z)qr + \left[\frac{I_x - I_y}{I'_z} + I_{xz}I'_{xz}\right]pq \tag{2.35}$$

$$I'_x = \frac{I_x I_z - I_{xz}^2}{I_z} \tag{2.36}$$

$$I'_z = \frac{I_x I_z - I_{xz}^2}{I_x} \tag{2.37}$$

$$I'_{xz} = \frac{I_{xz}}{I_x I_z - I_{xz}^2} \tag{2.38}$$

$$\frac{du}{dt} = \frac{X}{m} \tag{2.39}$$
$$\frac{dv}{dt} = \frac{Y}{m} \tag{2.40}$$
$$\frac{dw}{dt} = \frac{Z}{m} - g \tag{2.41}$$

$$\frac{dx}{dt} = u \tag{2.42}$$
$$\frac{dy}{dt} = v \tag{2.43}$$
$$\frac{dz}{dt} = w \tag{2.44}$$
$$\tag{2.45}$$

Taking into account equation 2.13 and all the equations above, the final derivative vector is:

$$\frac{d\mathbf{U}}{dt} = f(\mathbf{U}) \tag{2.46}$$

where $f(\mathbf{U})$ is equal to all the right hands sides of the equations above mentioned.

The equation used to integrate all of the variables is equation 2.19.

It needs to be remembered that the quaternion is a unitary vector so after each integration, its modulus requires to be set to 1 again (see equation 2.17).

5. **Rotational matrix:** This matrix can be easily computed once the quaternion is known. The equation that must be followed is 2.15 of section 2.2.

CHAPTER

THREE

Validation

3.1 Parabolic Shot

The first case carried out with the aim of checking if the results given by the code are correct is a simple parabolic shot. An initial velocity of the center of gravity on the X direction (u_0) is selected. The object is going to be subjected to free fall conditions, therefore the only force felt by the body is the force of gravity ($weight$).

The analytical solution of this problem is trivial. It gives to possibility of evaluating the answer given by the code with respect to the exact solution. The motion of a body performing a parabolic shot can be defined from the integration of Second Newton's Law, taking into account determined initial conditions ($x(t = 0) = 0$, $y(t = 0) = 0$ and $z(t = 0) = h_0$):

$$\begin{aligned} x(t) &= v_0 t \\ y(t) &= 0 \\ z(t) &= h_0 - \frac{1}{2} g t^2 \end{aligned} \tag{3.1}$$

As in this case all angular velocities and all moments are zero, there is no need to specify the body that it is used as the only thing that is interesting to compute is the movement of the center of gravity, no moments of inertia are involved.

Several tests are performed for this case. The simulation is run with different time steps and the behaviour of the error between the numerical results (x_n and z_n) and the analytical solution (x_a and z_a) is going to be evaluated. The error is defined as: $\epsilon_x = x_n - x_a$ and $\epsilon_z = z_n - z_a$. The error of the entire motion is computed as: $\epsilon = \sqrt{\epsilon_x^2 + \epsilon_z^2}$. However, after computing the motion, it is seen that ϵ_x is six order of magnitude smaller than ϵ_z. So, from now on, only the ϵ_z is going to be considered.

Firstly, the code is run until a certain final time and it is seen how the numerical final solution is deviated when compared with the analytical answer for different time step sizes, as shown in figure 3.1.

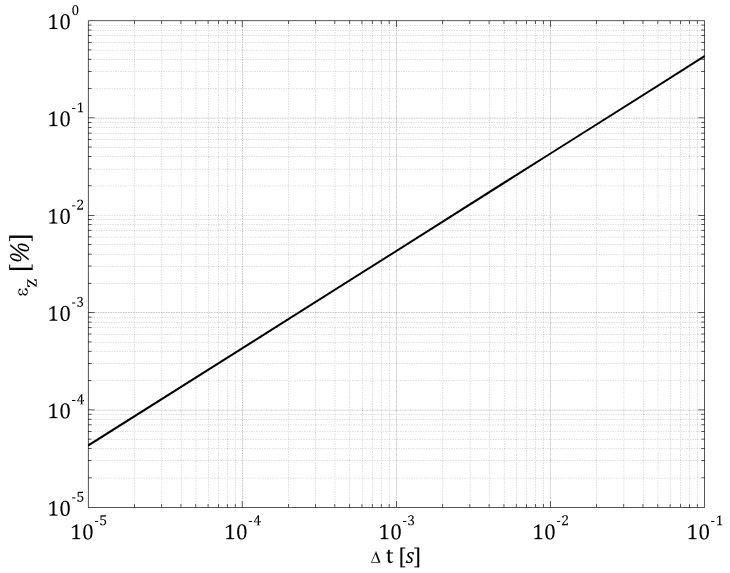

Figure 3.1: Error between analytical and numerical solutions after $t = 10s$ for different Δt

It can be seen that the line of figure 3.1 follows a power law of order 2 that is reasonable taking into account that the numerical scheme used is a second order method.

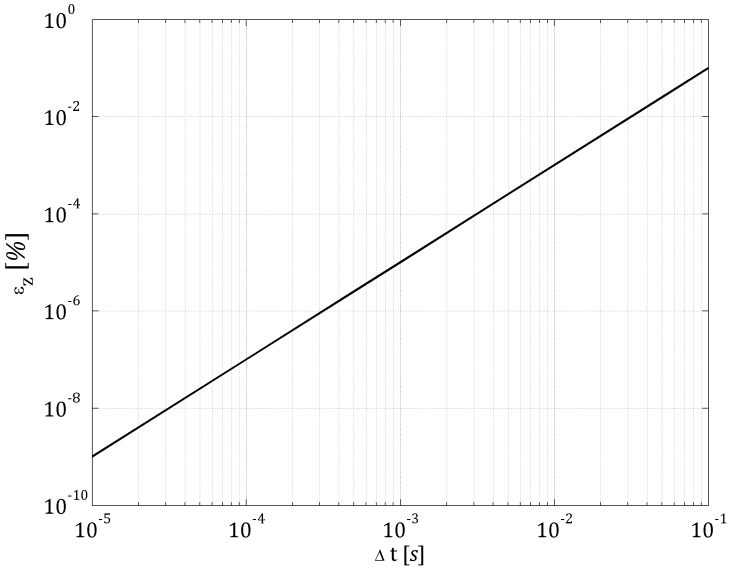

Figure 3.2: Error between analytical and numerical solutions at $t = \Delta t$ for different Δt

Another test that is done is to see what the error is after just one time step. It can be appreciated in figure 3.2 that the variation of the error and the size of the time step is also a power law of order 2 as in figure 3.1.

3.2 Axisymmetric problem of spacecraft

This is a problem taken from [14]. It involves the rotational motion of an spacecraft that possesses an axis of symmetry. The body used in the code is a cylinder with the Z axis being the axis of rotation whose tensor of inertia is:

$$\mathsf{I} = \begin{pmatrix} \frac{1}{12}m(3r^2+h^2) & 0 & 0 \\ 0 & \frac{1}{12}m(3r^2+h^2) & 0 \\ 0 & 0 & \frac{1}{2}mr^2 \end{pmatrix} \tag{3.2}$$

where m is the mass of the body, r is the radius of the cylinder and h is the height of the cylinder.

If the Z axis is chosen as the axis of symmetry of the body, a state of equilibrium for the spacecraft compromises a *pure spin* around that axis. So that $\omega_z = constant$ while $\omega_x = \omega_y = 0$. Let us introduce a initial disturbance ($\omega_x(0)$ and $\omega_y(0)$) in the last two variables. If this is executed, then the equations related to the angular velocities as a function of time are the following:

$$\begin{aligned} \omega_x(t) = &\quad \omega_x(0)\cos(kt) - \omega_y(0)\sin(kt) \\ \omega_y(t) = &\quad \omega_x(0)\sin(kt) + \omega_y(0)\cos(kt) \end{aligned} \tag{3.3}$$

where $k = \omega_z \frac{I_z - I_x}{I_x}$.

This implies an oscillatory movement in the XY plane while the z component (ω_z) remains unchanged. Consequently, the coming equation must be fulfilled:

$$\omega_{xy}^2 = \omega_x^2 + \omega_y^2 = \omega_x^2(0) + \omega_y^2(0) = constant \tag{3.4}$$

This constant lateral angular velocity ω_{xy} is responsible for the coning motion called *precession*. As this parameter is only dependent on the initial disturbance, it can be said that the motion is *"unconditionally stable"*.

Looking at figure 3.3, it is seen that the numerical and the analytical solutions are quite similar. The error of a variable is determined as the difference between the numerical and the analytical results normalized with the maximum values taken by the variable according to the analytical solution ($\epsilon_q = \frac{q_n - q_a}{q_{a_{max}}}$)). In figure 3.4, it can be appreciated the evolution of the error with respect to time for different time step sizes.

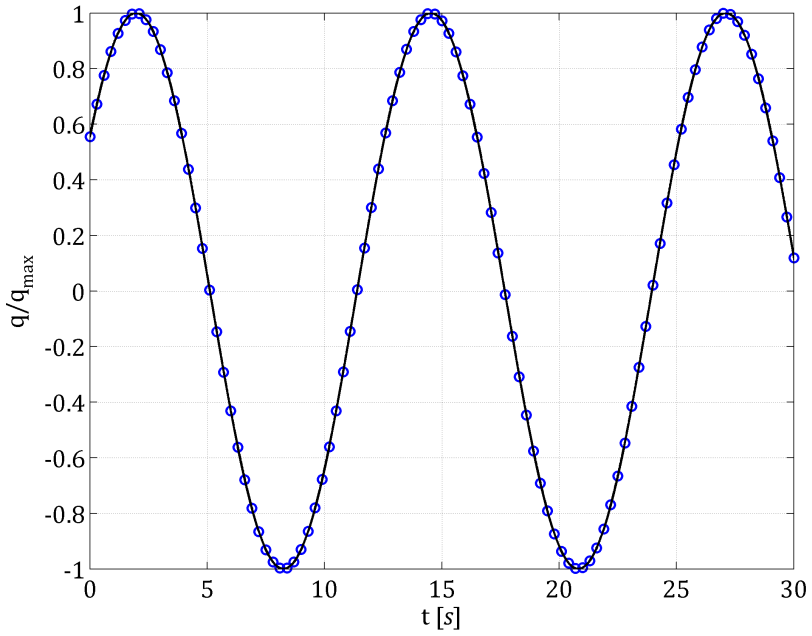

Figure 3.3: Plot of the analytical solution (—) and the numerical results (○ ○ ○) for $\Delta t = 0.001s$

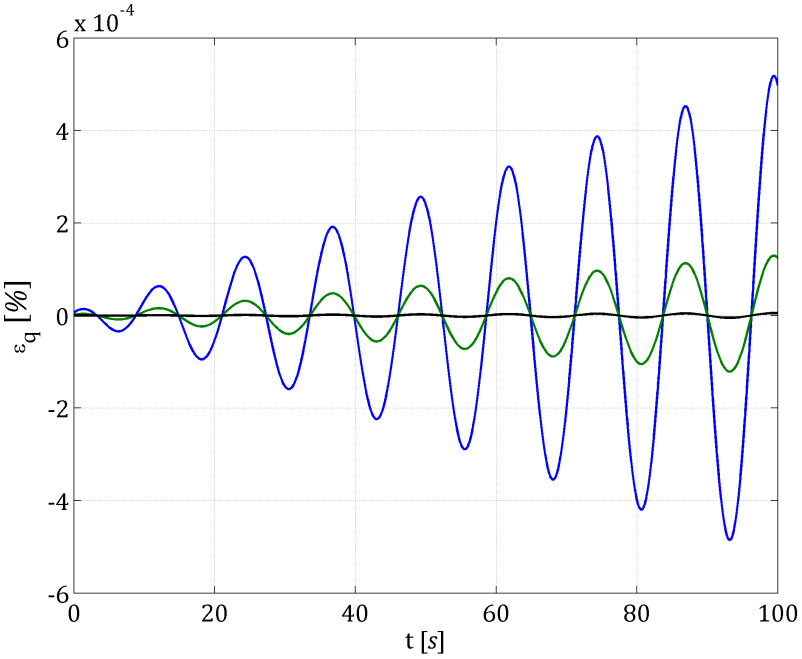

Figure 3.4: Comparison of the pitching velocity for $\Delta t = 0.001s$ (—), $\Delta t = 0.0001s$ (—) and $\Delta t = 0.00001s$ (—)

In figure 3.4, it is appreciated that the results obtained with *DyMoFlaps* are divergent. It means that the error will increase as time goes by due to the numerical error. In order to make this problem as small as possible, the size of the time step chosen should be as small as possible. In order to keep the computational time to reasonable expenses, a suitable time step size is $\Delta t = 0.001\ s$ that leads to an error less than 10^{-5} after 100 seconds.

Another study performed consists on looking at the error of the results after only one iteration. This last test gives the solution in figure 3.5 which is quite similar to the one obtained in figure 3.2. The slope of the line is approximately equal to a second power law, which correlates with the numerical method used.

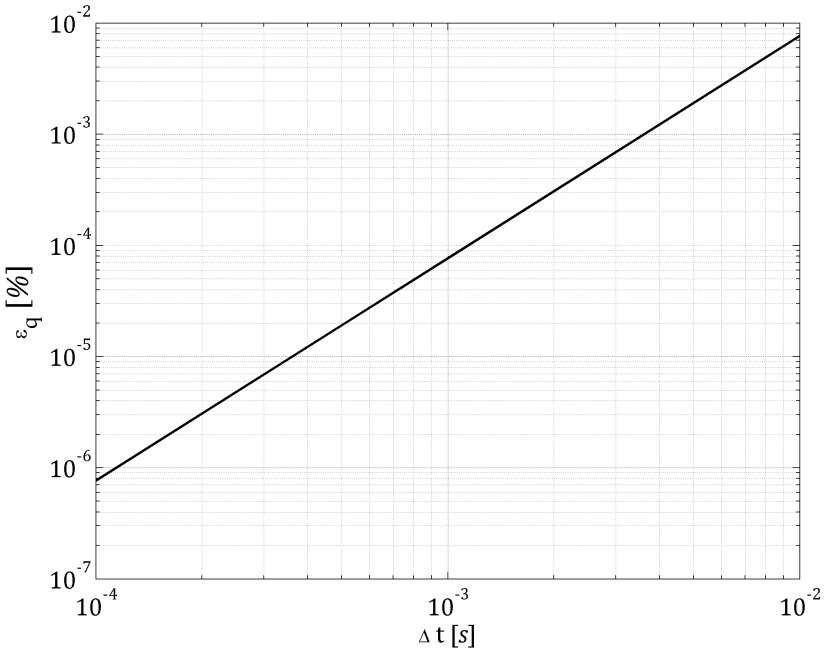

Figure 3.5: Error computed after the first time step as time step size is varied

3.3 Normal modes of the aircraft

In order to do the final validation test for *DyMoFlaps*, it was decided that a simulation of a real aircraft should be performed using the aerodynamic method described in section sec:AeroCode1.

The aircraft chosen for this test is the Lockheed Jetstar whose stability derivatives can be found in [16]. For more information about these data and how to compute the forces, please refer to appendix A.

This aircraft is a business jet from the 60's - 70's with a swept wing and a cruciform tail. In order to study its behavior, simulations will be performed in Matlab for a specific flight condition. In the scenario given, the aircraft will be at sea level ($h = 0\ m$) and will fly at a Mach number of $M = 0.4$.

The main scope of this section is to examine how well *DyMoFlaps* resembles the motion of the aircraft. The results are going to be compared with the obtained by means of the linearized analysis for the longitudinal case. The lateral case is more complex as it also excites the longitudinal magnitudes. Therefore the solution is not going to be linear but rather non linear.

The equations of motion for this second code are going to be integrated using a defined integrating function in Matlab called *ode45*. The rotations of the second code are going to be given by Euler angles. It needs to be borne in mind that the initial conditions used to excite the modes of the aircraft are sufficiently small so that the linear approach and DyMoFlaps have similar solutions. In principle, if the perturbations in the initial conditions were significantly large, the response of the two codes could be different due to the non-linear effects.

3.3.1 Longitudinal stability

In this first section, the aircraft response to longitudinal perturbations is going to be studied. In order to do so, the longitudinal modes of vibration have to be calculated to excite them and study how well these perturbations experienced by the aircraft are assessed. For this purpose a set of linearized equations to model dynamically the aircraft is applied ($\dot{\boldsymbol{x}} = A\mathbf{x}$), where $\dot{\boldsymbol{x}}$ are the variations of the set of variables $\mathbf{x}$ and A is the system matrix that determines the behaviour followed by the aircraft. This matrix is described by Etkin [15] and it is shown next:

$$\begin{bmatrix} \Delta\dot{u} \\ \dot{w} \\ \dot{q} \\ \Delta\dot{\theta} \end{bmatrix} = \begin{bmatrix} \frac{X_u}{m} & \frac{X_w}{m} & 0 & -g\cos(\theta_0) \\ \frac{Z_u}{m-Z_{\dot{w}}} & \frac{Z_w}{m-Z_{\dot{w}}} & \frac{Z_u - mu_0}{m-Z_{\dot{w}}} & -\frac{mg\sin\theta_0}{m-Z_{\dot{w}}} \\ \frac{1}{I_y}\left[M_u + \frac{M_{\dot{w}}Z_u}{m-Z_{\dot{w}}}\right] & \frac{1}{I_y}\left[M_w + \frac{M_{\dot{w}}Z_u}{m-Z_{\dot{w}}}\right] & \frac{1}{I_y}\left[M_q + \frac{M_{\dot{w}}(mu_0)}{m-Z_{\dot{w}}}\right] & -\frac{M_{\dot{w}}mg\sin\theta_0}{I_y(m-Z_{\dot{w}})} \\ 0 & 0 & 1 & 0 \end{bmatrix} \begin{bmatrix} \Delta u \\ w \\ q \\ \Delta\theta \end{bmatrix} \tag{3.5}$$

The two longitudinal modes that aircraft undergo are called phugoid and short period. The first one is characterized as a slow motion with a large period because of its small damping ratio and a small frequency of oscillation. In contrast the short period, as its name points out, has a small period; therefore larger damping and a greater frequency. Both of them will be stable if the real part of the eigenvalue is negative. This means that when suffering these perturbations, the aircraft will be able to return to its trim conditions.

The initial conditions are taken from the values of the eigenvector of the system matrix A. This is also the case for the lateral initial conditions of next section.

In order to calculate the system matrix coming from [15], the non-dimensional stability derivatives and then the dimensional values (see appendix A) are calculated. The modes of vibrations are given by the eigenvalues of this system matrix. Two pair of complex conjugates are obtained: $\lambda_{SP} = -0.7026 \pm 2.4196i$ and $\lambda_{PH} = -0.0043 \pm 0.0773i$.

The phugoid mode results obtained are the results that are going to be presented here. For the resolution of the short period, please refer to appendix B.

The comparison of the phugoid mode following this linear approach and with *DyMoFlaps* is seen to be quite close in figure 3.6. Taking a look to the difference between the values at each time step, the error is of the order of 10^{-4} as shown in figure 3.7. This error is defined as the difference between *DyMoFlaps* (u_D) and the linear approach (u_L) normalized by the initial free stream of the system (u_0). So this yields the following formula: $\epsilon_u = \frac{u_D - u_L}{u_0}$.

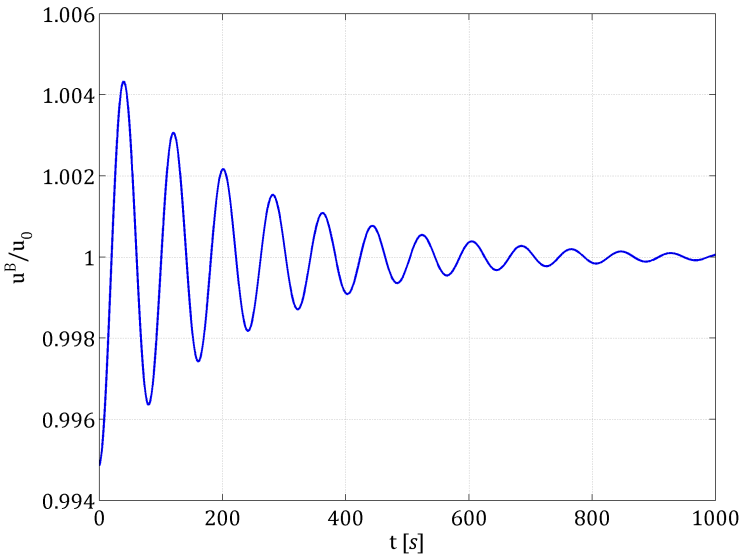

Figure 3.6: Phugoid mode result of the velocity on the direction of the x body axis, for the Matlab linear approach and *DyMoFlaps*

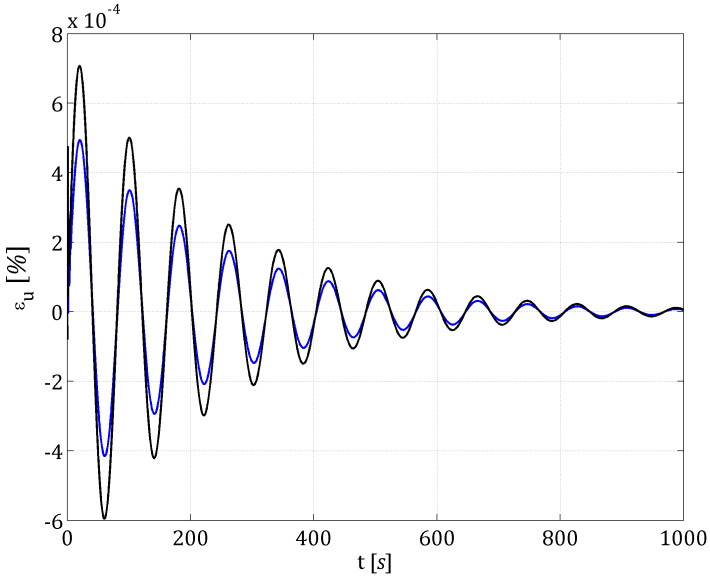

Figure 3.7: Short period error in u between the two codes for different time step sizes, $\Delta t = 0.001\ s$ (—) and $\Delta t = 0.0001\ s$ (—)

The above graphs show the variations in the free stream velocity due to the phugoid mode. When the aircraft is excited by the phugoid mode, the most important perturbations are suffered by the forward velocity and the elevation angle. When the system is excited by the short period, the significant magnitudes are the upward velocity and the elevation angle, too.

Figure 3.7 shows that the code can correctly simulate the phugoid mode with small errors after a long time. The error of the results obtained by the linearization method and by *DyMoFlaps* is not significant. Due to the different numerical methods applied to integrate the equations of motions, especially at the beginning, the error is larger. However it is reduced while the body evolves.

It is noticed that at the time step size decreses, the error decreases. However the change is very small. Between $\Delta t = 0.0001\ s$ and $\Delta t = 0.00001\ s$ the error is imperceptible.

3.3.2 Lateral stability

Moving on to lateral motion, modes of vibration in this direction will be studied. The system matrix has to be recalculated to match the lateral values and also different stability derivatives are needed:

$$\begin{bmatrix} \dot{v} \\ \dot{p} \\ \dot{r} \\ \dot{\phi} \end{bmatrix} = \begin{bmatrix} \frac{Y_v}{m} & \frac{Y_p}{m} & (\frac{Y_r}{m} - u_0) & g\cos(\theta_0) \\ (\frac{L_v}{I'_x} + I'_{xz}N_v) & (\frac{L_p}{I'_x} + I'_{xz}N_p) & (\frac{L_r}{I'_x} + I'_{xz}N_r) & 0 \\ (I'_{zx}L_v + \frac{N_v}{I'_z}) & (I'_{zx}L_p + \frac{N_p}{I'_z}) & (I'_{zx}L_r + \frac{N_r}{I'_z}) & 0 \\ 0 & 1 & \tan(\theta_0) & 0 \end{bmatrix} \begin{bmatrix} v \\ p \\ r \\ \phi \end{bmatrix} \tag{3.6}$$

where the expressions for I'_x, I'_z and $I'_{xz} = I'_{zx}$ are equations 2.36, 2.37 and 2.38.

In the lateral analysis, three modes of vibration appear. Rolling convergence mode ($\lambda = -0.0367$) and spiral mode ($\lambda = -2.687$) will be identified as the eigenvalues with real part only, which means they do not oscillate (*overdamped*). The pair of complex conjugates that is obtained is identified as the Dutch roll mode ($\lambda = -0.2798 \pm 2.6932i$). Since the real parts of the eigenvalues obtained are negative also for lateral modes, at first glance, the aircraft under study will recover from these perturbations, it is stable.

The Dutch roll motion is going to be represented here as an example from the lateral modes, the behaviour of the rolling convergence and spiral mode can be found in appendix B. The graph 3.8 shows the evolution of the variations of the lateral magnitudes. It can be appreciated that under the excitation of the Dutch roll mode, the aircraft recovers stability after some oscillations. It can be noticed that there is a coupled interaction between yawing and rolling moments. The changes suffered in this mode are small, where the lateral velocity is the most noteworthy change.

The error of figure 3.9 is selected as the difference between *DyMoFlaps* (v_D) and the nonlinear approach (v_{NL}) normalized by the maximum value of the lateral velocity for the nonlinear approach in absolute value ($v_{max} = |v_{max}|$). So this yields the following formula: $\epsilon_v = \frac{v_D - v_{NL}}{v_{max}}$.

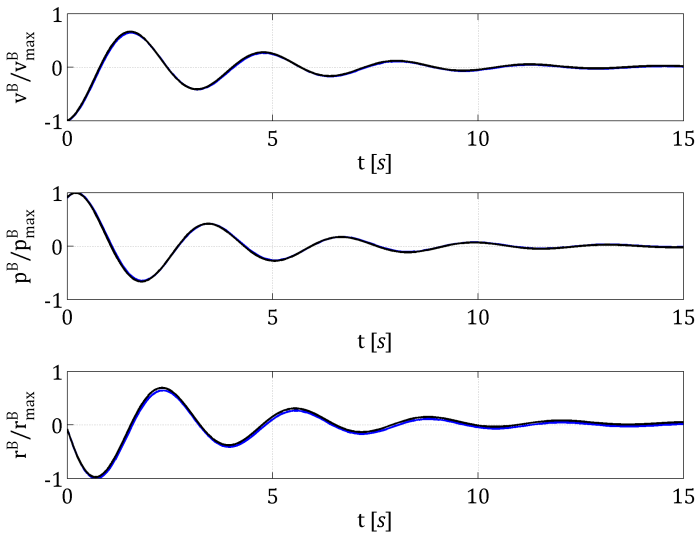

Figure 3.8: Dutch roll history of the lateral velocity and the roll and yaw rates for the Matlab integration (—) and *DyMoFlaps* (—)

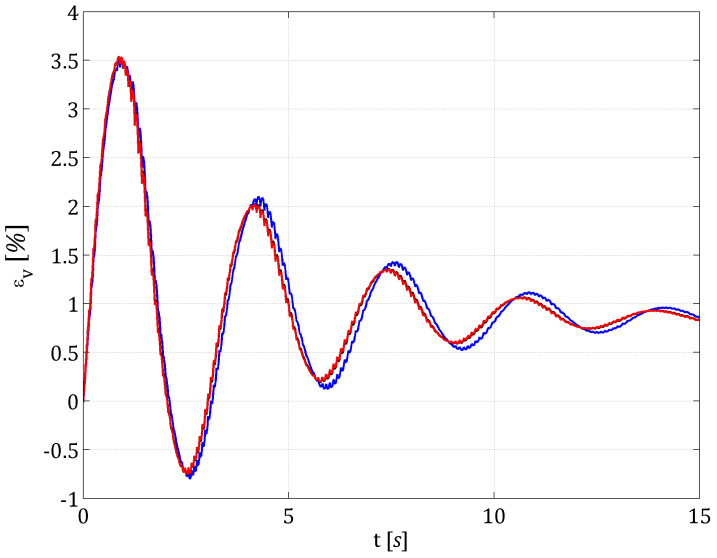

Figure 3.9: Dutch roll error between the lateral velocity solutions for $\Delta t = 0.001\ s$ (—), $\Delta t = 0.0001\ s$ (—) and $\Delta t = 0.00001\ s$ (—)

It is also seen that the longitudinal variables (u, w, p, θ) changes with this lateral excitation. This confirms the hypothesis explained at the beginning of this section where it was explained that a linear resolution where it was supposed that only the lateral modes were influenced is not correct. The orders of magnitude of the variations are different for each mode. However the differences in order of magnitude between the lateral and the longitudinal responses are in every case around three orders less for the longitudinal variables.

The error is observed to be greater for the lateral velocity that for the two angular rates. This happens as a consequence of the higher values of velocity that the aircraft undergoes. As the velocity in the stream wise direction is approximately $u = 136\ m/s$, a small variation of the yaw angle will create prominent variations on the lateral velocity (v). The error in any case can be considered small.

CHAPTER

FOUR

Results

4.1 Problem definition

The motion of a glider is going to be studied. Gliding involves an unpowered ($T = 0$) motion through a fluid. The aircraft will describe a descending trajectory with a fixed path angle (γ). This angle depends on the aerodynamic efficiency (L/D) of the glider:

$$\begin{cases} L = W\cos\gamma \\ D = W\sin\gamma \end{cases} \Rightarrow \tan\gamma = \frac{1}{L/D} \tag{4.1}$$

Once the steady state is reached, the velocities will be constant as the forces cancel each other so there is no acceleration. The lift generated during this arrangement should remain approximately constant, therefore the drag generated by the motion should not change also. However, as the temporal response is going to be analyzed, there will be a non-stationary region at the beginning of the motion where oscillations of the variables occur.

It is worth mentioning that if, instead of a fixed wing, a flapping wing motion is imposed, thrust could be achieved and so the flight will not be a gliding motion and it could become a steady level flight.

The dynamic evolution in all cases is computed by *DyMoFlaps*, using different approaches for the aerodynamic forces that can be handled as coefficients in order to achieve non-dimensional parameters. The ones that should be tuned for a longitudinal motion are: the lift coefficient (C_L), the drag coefficient (C_D) and the pitching moment coefficient (C_M). These coefficients are defined as:

$$C_L = \frac{L}{\frac{1}{2}\rho v_T^2 S} \tag{4.2}$$

$$C_D = \frac{D}{\frac{1}{2}\rho v_T^2 S} \tag{4.3}$$

$$C_M = \frac{M}{\frac{1}{2}\rho v_T^2 S c} \tag{4.4}$$

where ρ is the density of the air at sea level conditions, $v_T^2 = u^2 + v^2 + w^2$ is the total speed, S represents the wing surface and c is the chord of the wing.

4.2 Aerodynamic analysis

The aerodynamic forces and moments that are applied to the body are going to be computed according to the two different methods explained in 2.4:

- Firstly, the same code used to compute the development of the natural modes of the aircraft with the integrating function *ode*45 is going to be used (*option 1*). That means that the forces and moments are the linearized approximation of the real forces. This can only be applied to fixed wings.
- The second procedure to calculate the forces generated is by means of the aerodynamic Matlab code (*option 2*). This code can compute forces for fixed and flapping wings.

Notice that the drone does not have the same wing and tail configuration for both aerodynamic options. For the first one the lifting surfaces (wing and tail) are both taken from XFLR5. Yet in the second option the wing is composed of panels to compute the forces with the aerodynamic code of *option 2* while the tail is estimated with linear aerodynamics. So the modeling of the two options is different. In order to have approximately the same solution using the different aerodynamic approaches, the three aerodynamic coefficients (C_L, C_D and C_M) should remain constant for all cases. For this to be possible, a preliminary study is going to be performed approximating linearly the coefficients of lift and pitching moment. The aim is to achieve at equilibrium conditions, the same coefficients for *option 2* as the ones given by *option 1*.

These coefficients (C_L and C_M) when linearized are usually said to depend also on the free stream velocity (u), the pitching rate (q) and the change in angle of attack ($\dot{\alpha}$). However, for the basic results performed in this project, it is only going to be considered the effect of the angle of attack that is the most significant. So the lift coefficient is the sum of the lift coefficient at zero angle of attack ($C_{L_0} = C_L(\alpha = 0°)$) and the influence of α in the lift coefficient (C_{L_α}), same reasoning can be done for the moment coefficient:

$$C_L = C_{L_0} + C_{L_\alpha}\alpha \tag{4.5}$$

$$C_M = C_{M_0} + C_{M_\alpha}\alpha \tag{4.6}$$

The angle of attack is defined as the addition of the angle between the free stream and the x body axis and the angle of installation of either wing and tail ($\alpha = \arctan\frac{w_B}{u_B} + \alpha_I$). The angle of installation is positive as seen in figure 4.1.

The definition of the C_{L_0} for the aerodynamic study 2 differs from the one that can be computed for the linearized forces (*option 1*). In this linearized option, the $C^*_{L_0}$ is given by the lift at the reference condition of choosing, in this case $L = mg$. This must be kept in mind so that when the movement is initiated, the body in the simulation with the panel method (*option 2*) should start with an initial angle

of attack α_B to give the same lift as the reference condition of the linearized case. From XFLR5 it is obtained that the angle of attack that the wing should have in order to have its lift equal to the weight and also the sum of moments equal to zero at $u = 20\ m/s$ is $\alpha_{eq} = 1.123°$.

Now that the coefficients have been explained and linearized, the adjustments that need to be done in order to keep constant the values of the coefficient for both aerodynamic approaches is going to be discussed. On the one hand, the lift and moment coefficient are going to be studied. On the other hand, the different approaches used for the drag coefficient are presented.

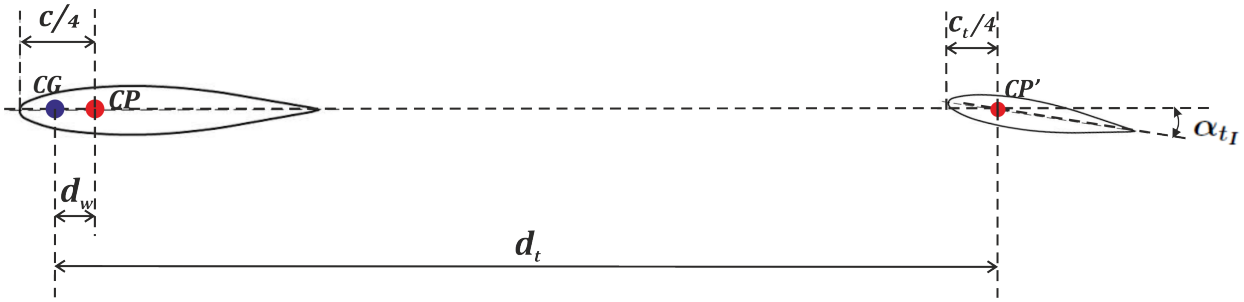

Figure 4.1: Layout of the wing-tail configuration

4.2.1 Lift and pitching moment coefficients

The lift coefficient for aerodynamic *option 1*, as previously said, has a reference $C^*_{L_0}$. In order to achieve this conditions when applying the second aerodynamic option, the drone is rotated an initial angle $\theta_0 = \alpha_0 = \frac{C^*_{L_0}}{C_{L_\alpha}}$ that should be similar to the angle of attack at equilibrium conditions, $\alpha_{eq} = 1.123°$. The value of this angle is found to be $\theta_0 = 1.66°$, which is in fact close to α_{eq}.

Apart from the previous operation that must be done in order to achieve the same initial C_L, the lift coefficient depends highly on the wing, that has the same geometry for both options. Hence, the C_{L_α} is the same for both options. This also means that the installation angle of the wing should be $\alpha_{w_I} = 0$ not to modify the lift coefficient.

Regarding the pitching moment calculations, in order for the aircraft to be stable and be able to fly, the sum of the moments should be equal to zero. At this moment is when the effect of the tail becomes of great importance. The moment coefficient can be expressed as the sum of the moments created by the wing (C_{M_w}) and by the tail (C_{M_t}), the weight does not create any moment as it is directly applied in the center of gravity (CG), point with respect to the moments are taken. The equation of the moments at the center of gravity is:

$$C_{M_{CG}} = C_{M_w} + C_{M_t} = C^w_{M_{c/4}} - C^w_L d_w + C^t_{M_{c/4}} - C^t_L d_t \tag{4.7}$$

The nomenclature is:

$C^w_{M_{c/4}}$ - C_M of the wing at a quarter chord of the leading edge of the wing (CP)

C^w_L - C_L of the wing

d_w - Distance between the CG and the CP

$C^t_{M_{c/4}}$ - C_M of the tail at a quarter chord of the leading edge of the tail (CP_t)

C^t_L - C_L of the tail

d_t - Distance between the CG and the CP_t

Substituting the moment and lift coefficients by their linearized functions explained in equations 4.5 and 4.6 and setting $C_{M_{CG}} = 0$, equation 4.7 becomes a function of the angle of attack only. This angle of attack is divided in the angle of attack with respect to the body (α_B) and the angle of installation (α_{t_I}). The angle of attack wants to be kept to the value obtained from *option 1* to be at equilibrium at the same angle of attack so $\alpha_B = \alpha_{eq}$. Hence the only possibility to adjust the equation is by setting a specific value to the α_{t_I}. As the wings are designed as a flat plate (*option 2*) or a symmetric airfoil (*option 1*), the lift and the pitching moment at $\alpha = 0$ are zero ($C^w_{L_0} = C^w_{M_{0_{c/4}}} = C^t_{L_0} = C^t_{M_{0_{c/4}}} = 0$) for both aerodynamic approaches. The final equation is the following:

$$(C^w_{M_\alpha} - C^w_{L_\alpha} d_w)\alpha_B = (C^t_{L_\alpha} d_t - C^t_{M_\alpha})(\alpha_B + \alpha_{t_I}) \tag{4.8}$$

The value of the α_I of the tail (α_{t_I}) that needs to be accounted for is: $\alpha_{t_I} = -2.58°$. Recalling the data from the drone that was selected for the simulation in XFLR5, the installation angle should be $\alpha_{t_I} = -1°$. The down-wash that is created is the principal reason why the installation angle of the tail should be changed for the sum of moments to be zero at $\alpha_B = \alpha_{eq}$. This difference between the two models comes from the assumption when proceeding with the panel method (*option 2*) that the wing is not influenced by the wake created by the wing. Due to the fact that the tail is not been affected by the wake, no down-wash angle is produced.

4.2.2 Drag coefficient

The drag coefficient is more complex to estimate with a potential method as viscous effects are not taken into account. So part of the drag, the parasite drag, cannot be computed easily. In XFLR5 this part of the drag can be estimated. However the other component of the drag that is contemplated in this project is the induced drag that is dependent on the lift generated. This part of the drag can indeed be estimated in *option 2* but, in order to do so, more hypothesis must be taken into account. These calculations are based in [20], with a modification to take into account the incident velocities different from the free stream.

At the end the drag coefficient is going to be estimated in two different ways also:

- The first tests are performed with a fixed drag coefficient that is: $C_D = C_{D_0} + C_{D_i}$. The parasite drag C_{D_0} and the induced drag C_{D_i} values are taken from [18] where the induced drag is the one that the wing of XFLR5 has for equilibrium conditions ($L = mg$ and $M = 0$).
- For the second part, the value of parasite drag is kept while the value of the induced drag is computed by the aerodynamic panel method code (*option 2*).

4.3 Cases of study

Cases are going to be run for a wing fixed to the body and also for flapping wings. The flapping wing will describe a heaving motion with different amplitudes (h_0). The heaving frequency ($f = \frac{\omega}{2\pi}$) is kept constant and equal to $f = 0.25Hz$.So finally the set of cases that are going to be studied are shown in table 4.1.

For a fixed wing, there is no chance that the wing produces thrust instead of drag as said in section 1.2. However for a flapping wing thrust could by in principle achieved, as said in section 4.1. For a constant drag coefficient, the possibility of having a thrust force is not contemplated as the drag force is already imposed to be oriented to oppose the motion of the drone. Finally if $C_D \neq const$ and therefore the induced drag is computed by the code of *option 2* and so thrust may be produced for a flapping motion.

It is needed to keep in mind that the analysis of flapping wings is still considered "work in progress". The main objective of the simulations presented here for flapping wing configuration is to provide an idea of the opportunities that DyMoFlaps can bring. It is also a way to validate the integration of the aerodynamic unsteady panel method (see section 2.4.2) and the dynamic model.

	$h_0/c = 0$	$h_0/c = 0.02$	$h_0/c = 0.5$
$C_D = const$	Aero option 1 and 2 (section 4.4.1)	Aero option 2 (section 4.4.2)	Aero option 2 (section 4.4.2)
$C_D \neq const$	Aero option 2 (section 4.5.1)	Aero option 2 (section 4.5.2)	Aero option 2 (section 4.5.2)

Table 4.1: List of cases studied

4.4 Constant drag coefficient

4.4.1 Fixed wings & aerodynamic options 1 and 2

For option 1, the stability derivatives obtained from XFLR5 are used, see appendix C. The initial conditions of the motion (position, linear and angular velocities and Euler angles) are set to zero with the exception of the forward horizontal linear velocity that is $u = 20\ m/s$ in inertial axes. The aircraft using this approach is already at a reference condition that implies a rotation of an angle θ_0. So the initial conditions for option 1 are set with respect to the body axes already oriented as required from the reference conditions. The conditions expressed with respect to the inertial reference frame remain unchanged.

The initial conditions in this case for option 2 are similar. The only thing that changes is that now the body is rotated an angle θ_0 with respect to the Y body axis. Notice that this rotation does not mean that the aircraft for the first and the second option start the motion at different states. It is used to account for the already rotated body axes in option 1.

For the purpose of being consistent with the variables handled, all the results are going to be presented in body axes, not the *"reference"* body axes of option 1, or in inertial axes.

Three simulations are run:

- **Case 1:** Option 1 with the installation angle $\alpha_{t_I} = -1°$ (——)
- **Case 2:** Option 2 with the installation angle $\alpha_{t_I} = -1°$ (——)
- **Case 3:** Option 2 with the installation angle $\alpha_{t_I} = -2.58°$ (——)

Let us start by analyzing the behaviour of the forces for the three cases. The force coefficients shown in figures 4.2 and 4.3 are computed from the X and Z forces with respect to the inertial reference frame. It can be appreciated that the resultant force in inertial axis should only be a force in the Z direction that opposes the weight of the aircraft. So the X force oscillates around the zero value as seen in figure 4.3. The stationary value of the Z force coefficient is different for each of the cases. This is due to the fact that the angle of attack, expressed as the angle between the free stream and the X body axis, is different for each case as can be viewed in table 4.2. The greater the angle of attack (α_B), the higher the C_{Z^I} as this coefficient is mainly related to the lift coefficient of the aircraft.

Case	1	2	3
α_B [°]	1.6597	1.0602	2.7311
v_T $[m/s]$	19.9688	29.4283	18.6873
C_{z^B}	0.1216	0.0547	0.1392
C_{x^B}	0.0141	0.0135	0.0135
C_{z^I}	0.1225	0.0564	0.1398
C_{x^I}	0.0000	0.0000	0.0000
L/D	11.5430	3.7412	6.8660
$\gamma = atan(\frac{1}{L/D})$ [°]	4.9513	14.9650	8.2865
$\gamma = atan(\frac{w^I}{u^I})$ [°]	4.9500	14.9650	8.2865

Table 4.2: Stationary values for the three cases studied in this section

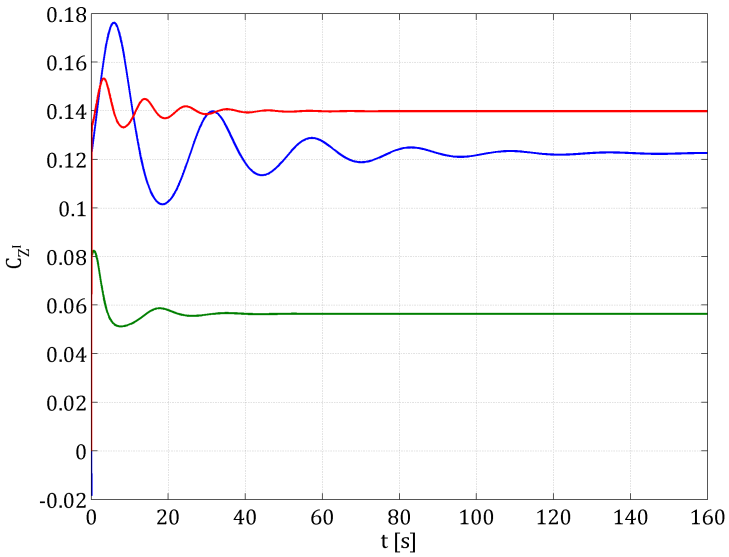

Figure 4.2: Z^I force coefficient for cases 1 (—), 2 (—) and 3 (—)

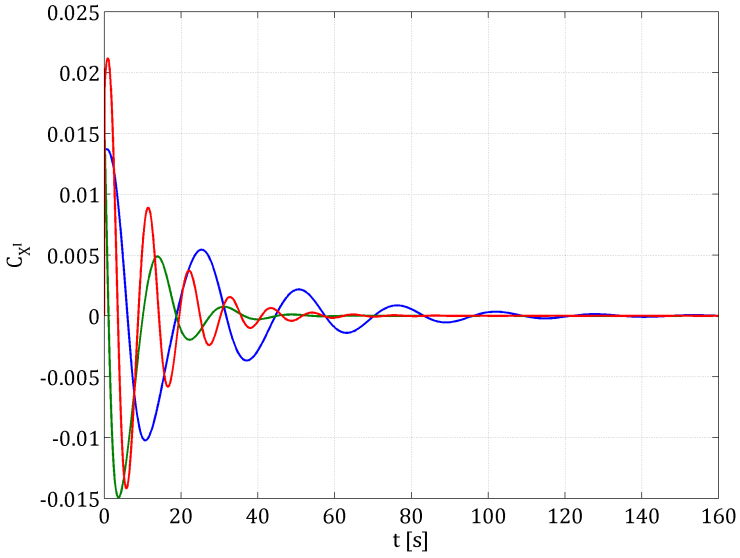

Figure 4.3: X^I force coefficient for cases 1 (—), 2 (—) and 3 (—)

As the lift coefficients at equilibrium conditions are different, the velocity at which the body needs to go to create sufficient lift to counteract the weight will be different. This is why the larger the C_L, the lower the forward velocity (u_B) needed as it can be seen in figure 4.4.

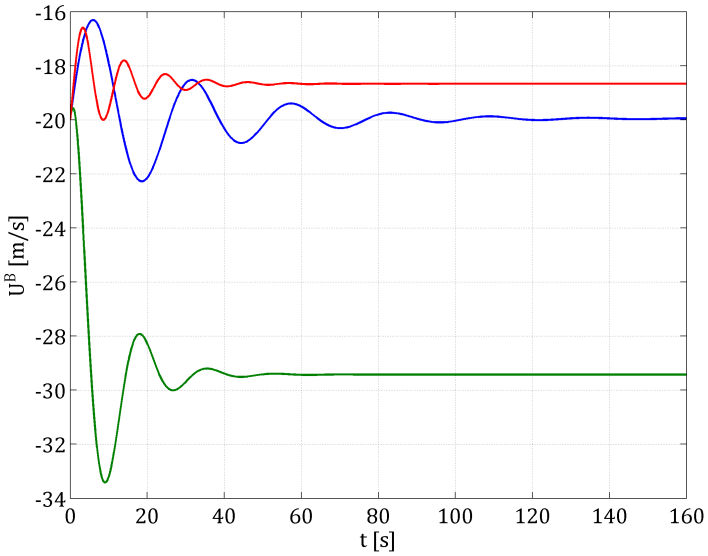

Figure 4.4: Forward velocity in body axes for cases 1 (—), 2 (—) and 3 (—)

From the previous figures, it can be appreciated that the frequency (f) of the oscillations for each case is different, being the greatest for case 3 and smallest for case 1. This also implies that the period (T) of the oscillation decrease from case 1 to case 3. In addition, the damping of each motion can be quantified by means of the settling time ($t_{settling}$). These parameters are defined as were the values of the curve stay between a tolerance range. The tolerance imposed for this calculations has been of 0.1 % of the stationary value. The settling time is the largest for case 1 and smallest for case 2. This characteristics can be seen in every figure of this section.

Case	1	2	3
T $[s]$	25.7004	17.6217	10.6711
f $[Hz]$	0.0389	0.0567	0.0937
$t_{settling}$ $[s]$	139.0444	54.4175	58.0369

Table 4.3: Parameter of the motion for the three cases studied

The path followed by the glider should be a line descending with a fixed angle called γ as it was explained at the beginning of this chapter. The resultant trajectories are plotted in figure 4.5.

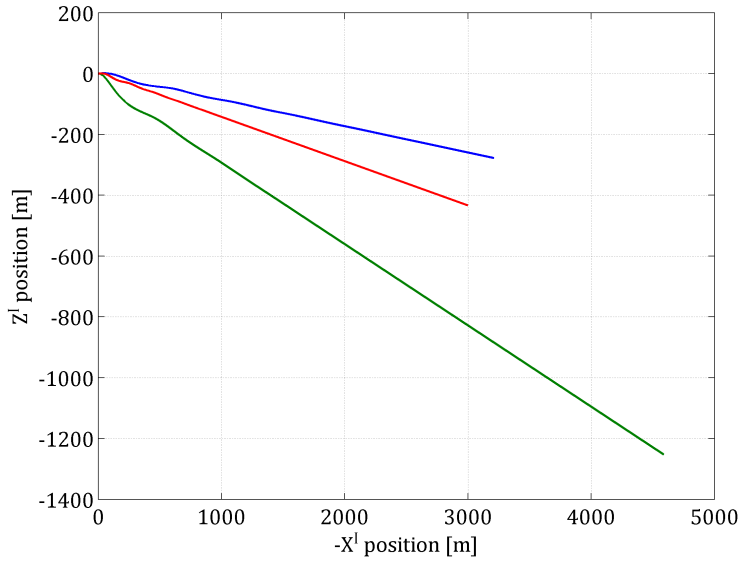

Figure 4.5: Trajectory followed by the glider for cases 1 (—), 2 (—) and 3 (—)

The path angle (γ) only depends of the value of the aerodynamic efficiency (L/D) as expressed in equation 4.1. The value of γ has been calculated in table 4.2 in two different ways. One of them is solved using equation 4.1. The other one accounts

for the fact that the path angle can be computed using the velocities of the CG in inertial axis:

$$\gamma = atan(\frac{w^I}{u^I}) \tag{4.9}$$

It can be seen in table 4.2 that the comparison of these two values for all cases is precise. The aerodynamic efficiency is observed to be greater for case 1 and the smallest for case 2. This can also be appreciated that the path angle in figure 4.5 is lower for case 1 and the greatest for case 2.

Moving on to the orientation of the drone while it descents, figure 4.6 represents the angle that the X body axis has with respect to the X inertial axis. It is defined as the difference between the angle of attack α_B and the path angle γ: $\beta = \alpha_B - \gamma$.

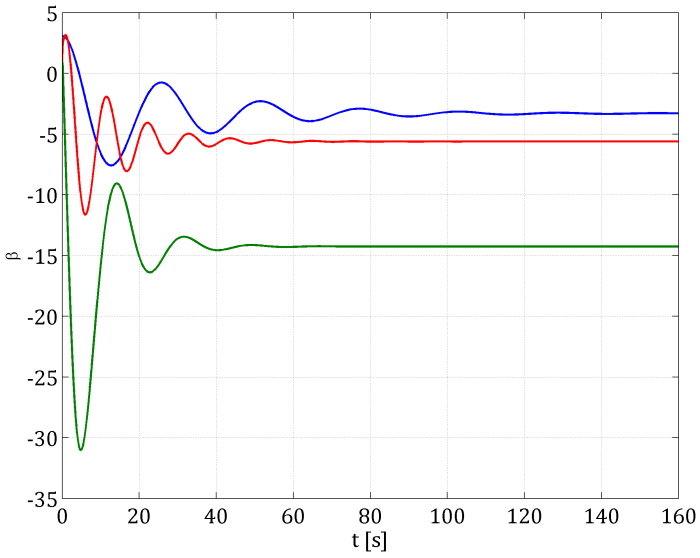

Figure 4.6: History of the orientation of the drone with respect to the ground (β) for cases 1 (—), 2 (—) and 3 (—)

The nose of the drone is pointing towards the ground for every case. It can be seen in figure 4.6 that the largest oscillation made by the glider occurs in case 2 where it goes beyond an angle $\beta = -30°$.

4.4.2 Flapping wings & aerodynamic option 2

The simulations in this section are performed for a heaving motion at two different heaving amplitudes. Due to the relative motion of the wing with respect to the body, an extra component of the angle of attack seen by the wing needs to be taken into account. The wing is moved up and down with a speed equal to:

$w_{flap} = h_0\omega\cos(\omega t)$ where ω is the frequency of the heaving motion, not the angular velocity [19].

As the change in vertical velocity on the wing is symmetric with respect to the body, the extra component of the angle of attack will be a sinusoidal curve with an amplitude dependent on the heaving amplitude h_0 and the heaving frequency ω. So all the oscillations are going to be greater for $h_0/c = 0.5$.

The simulations contrasted in this part are:

- **Case 1:** Fixed wing configuration with constant drag and $\alpha_{t_I} = -2.58°$ (——)
- **Case 2:** Flapping wing configuration with constant drag, $\alpha_{t_I} = -2.58°$ and a heaving amplitude $h_0 = 0.02c$ (——)
- **Case 3:** Flapping wing configuration with constant drag, $\alpha_{t_I} = -2.58°$ and a heaving amplitude $h_0 = 0.5c$ (——)

In figure 4.7, it is shown the change in the Z^I force coefficient. It can be appreciated that the difference between the previous case with fixed wings and the same conditions with flapping wings gives a different motion. The angle of attack will indeed change and so the lift coefficient will change periodically too. At the beginning of the motion, the changes produced by the flapping are more significant. However when the stationary is reached, the mean lift coefficient after one period is still very similar to the linear one hence the forward velocity u^B in figure 4.8 also changes periodically with a mean value equal to the one of the fixed wing.

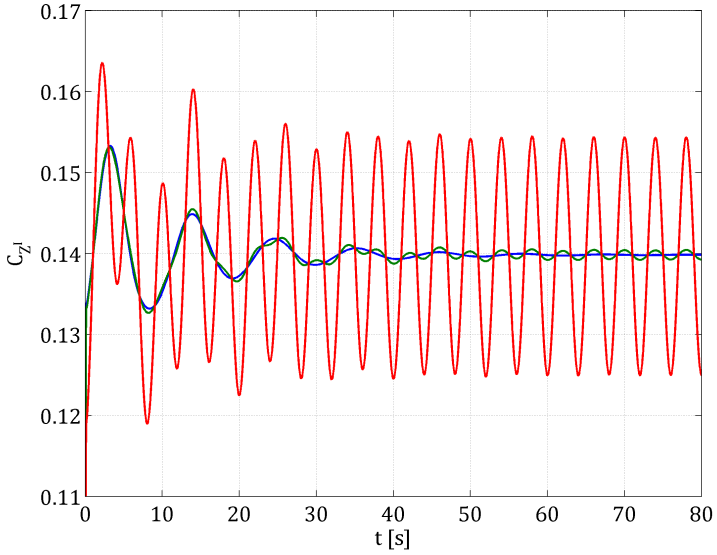

Figure 4.7: Z^I force coefficient for cases 1 (——), 2 (——) and 3 (——)

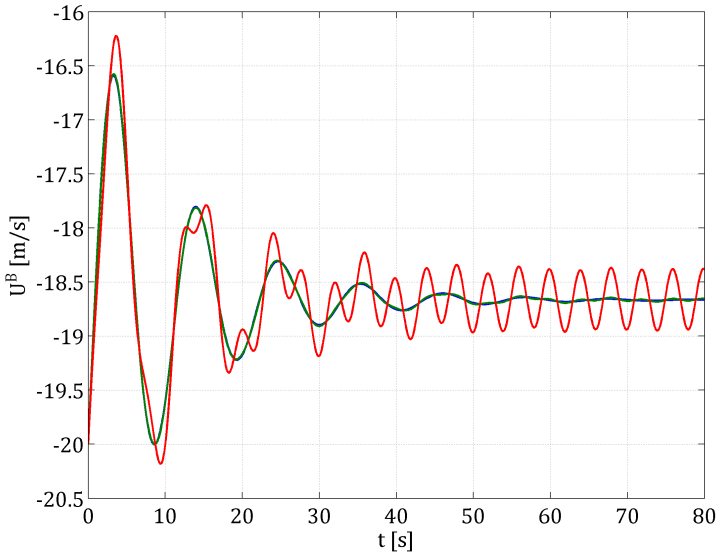

Figure 4.8: Forward velocity in body axes for cases 1 (—), 2 (—) and 3 (—)

Taking a look to figure 4.9, it can be seen that the X^I force coefficient is still tending to zero as it is the desired condition. Nevertheless, as the lift generated changes periodically, the resultant force in inertial axis will be perturbed too as one of its components is the projection of the lift onto the X^I axis.

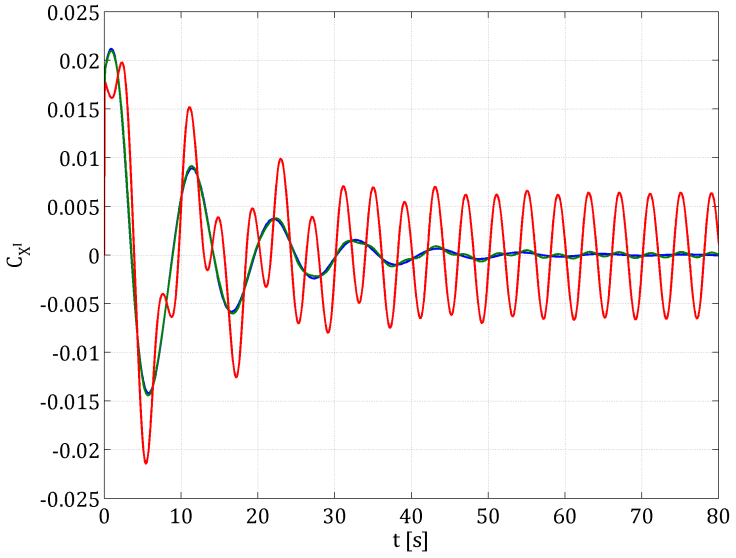

Figure 4.9: X^I force coefficient for cases 1 (—), 2 (—) and 3 (—)

Talking about the path angle followed by the trajectory of the flapping drone, there is not a notable change in figure 4.10. The mean lift coefficient is still the same and the drag coefficient has not been modified so the aerodynamic efficiency (L/D) has not change from section 4.4.1. So the drone descends at the same rate and with the same trajectory with fixed or flapping wings.

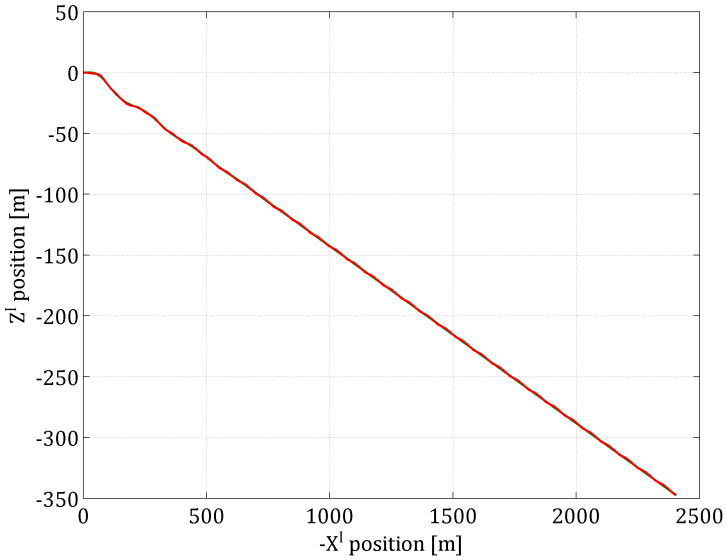

Figure 4.10: Trajectory followed by the glider for cases 1 (—), 2 (—) and 3 (—)

The orientation of the drone while it descents,as seen in figure 4.11, changes due to the change in angle of attack. The greatest change is, of course, experienced for flapping at a greater amplitude where $h_0/c = 0.5$ and the amplitude of the periodic oscillations is of 2.285°.

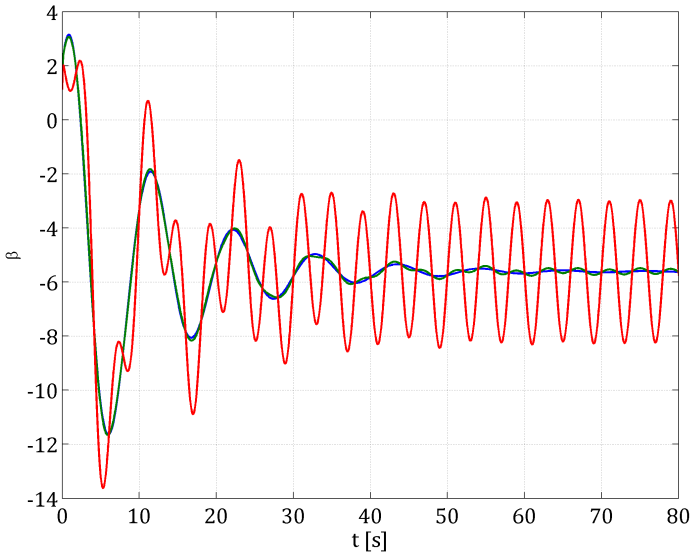

Figure 4.11: History of the orientation of the drone with respect to the ground (β) for cases 1 (—), 2 (—) and 3 (—)

4.5 Variable drag coefficient

4.5.1 Fixed wings & aerodynamic options 2

The case that is compared here is case 3 of section 4.4.1. This means that the angle of installation of the tail is $\alpha_{t_I} = 2.58°$. The results of section 4.4.1 are going to be compared with a simulation where the induced drag is computed from the aerodynamic code, so it will not be constant like in section 4.4.1.

The two cases compared in this subsection are:

- **Case 1:** Fixed wing configuration with constant drag and $\alpha_{t_I} = -2.58°$ (—)
- **Case 2:** Fixed wing configuration with variable drag and $\alpha_{t_I} = -2.58°$ (—)

In figure 4.12 the change perceived in the Z^I coefficient is not relevant, about a 0.42 % decrease of the stationary value for the inconstant C_D with respect to the stationary value for the constant C_D. This happens as a consequence of the drag projection component that this force coefficient has, even is the effect is meaningless as seen in figure 4.12. The lift coefficient remains unchanged in principle.

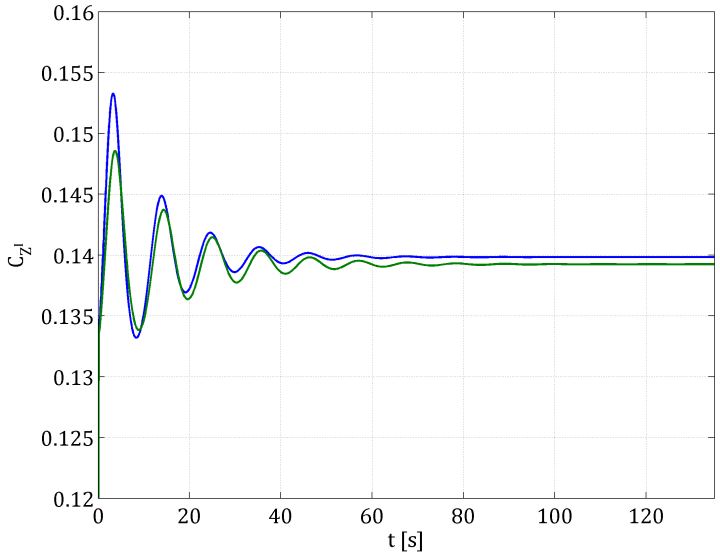

Figure 4.12: Z^I force coefficient for cases 1 (—) and 2 (—)

As a result of the small change in the force coefficient, the changes in the u^B velocity are also very small. This phenomenon can be appreciated in figure 4.13.

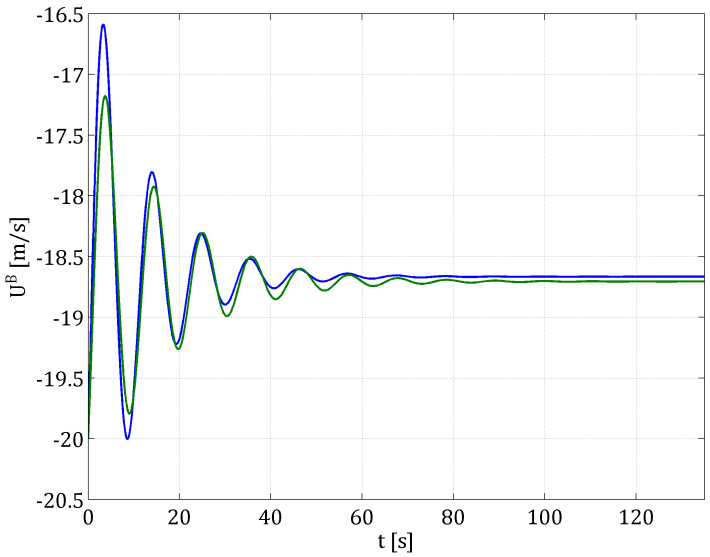

Figure 4.13: Forward velocity in body axes for cases 1 (—) and 2 (—)

The amplitude of the oscillations have decreased now that the drag coefficient is able to change, as can be appreciated in figure 4.14. The variations in the angle of attack will change consequently the drag coefficient. This implies reduction of the

drag coefficient, resulting from a α_B that gives an induced drag smaller than the one accounted for in section 4.4.1. However this results is not consistent with the fact that the angle of attack α_B that the drone is seeing is greater than the angle used to compute the induced drag for the constant drag approach. Naturally as the methods to estimate it are different, the result should not be the same. However the difference between the two appears to be more significant than expected. The computation of the induced drag by the aerodynamics of *option 2* is still in progress and so this should be taken as only a mere example of the prospects of what could be achieved by the integration of DyMoFlaps and *option 2*.

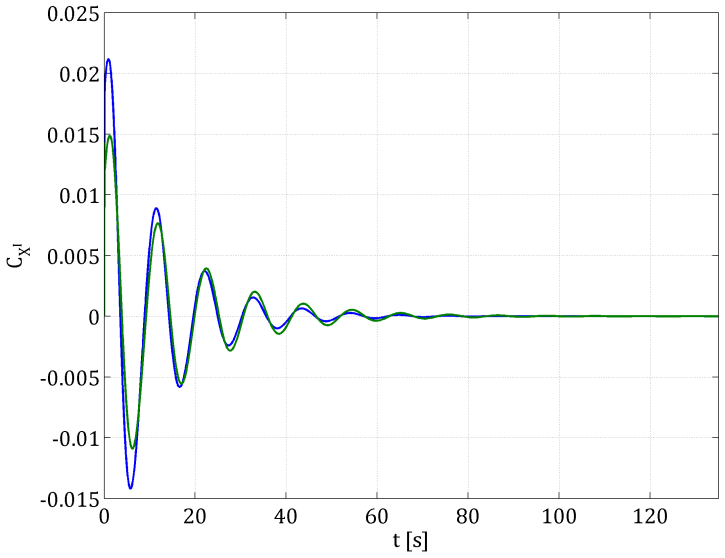

Figure 4.14: X^I force coefficient for cases 1 (—) and 2 (—)

In this case, the damping and the frequency of the oscillations are changed in the way shown in table 4.4. The parameter that it is most affected is the damping. The oscillations need more time for the case of $C_D \neq const$ to die out.

Case	$C_D = const$	$C_D \neq const$
$T\ [s]$	10.6711	10.6650
$f\ [Hz]$	0.0937	0.0938
$t_{settling}\ [s]$	58.0369	73.6406

Table 4.4: Parameter of the motion for the two cases of study in this section

The drag coefficient decrease indicates a change in the aerodynamic efficiency, making a noteworthy increase of this value (see table 4.4). Therefore the path angle followed by the case of $C_D \neq const$ is smaller, as in figure 4.15.

Case	$C_D = const$	$C_D \neq const$
α_B [°]	2.7311	2.7311
L/D	6.8660	10.9866
$\gamma = atan(\frac{1}{L/D})$ [°]	8.2865	5.2008
$\gamma = \frac{w^I}{u^I}$ [°]	8.2865	5.2008

Table 4.5: Stationary values for the two cases studied in this section

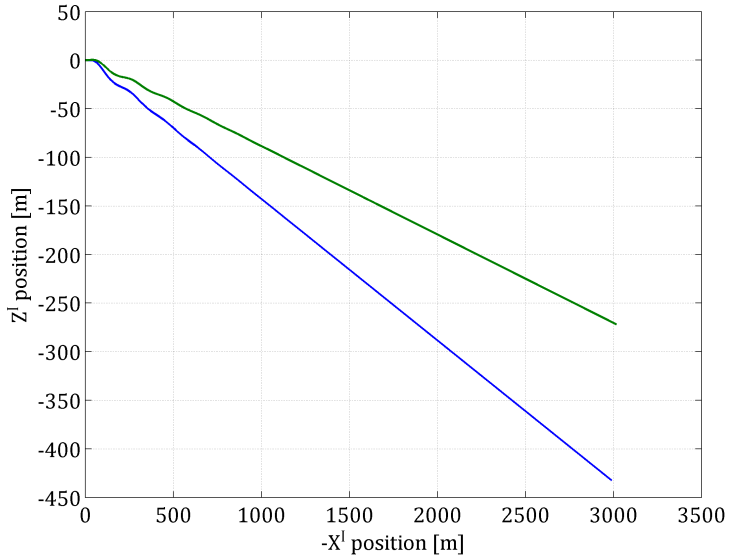

Figure 4.15: Trajectory followed by the glider for cases 1 (—) and 2 (—)

As the path angle γ has changed and the angle of attack of the wing remains approximately the same than for the case of $C_D = const$, the orientation angle β changes also. Its behaviour is plotted in figure 4.16.

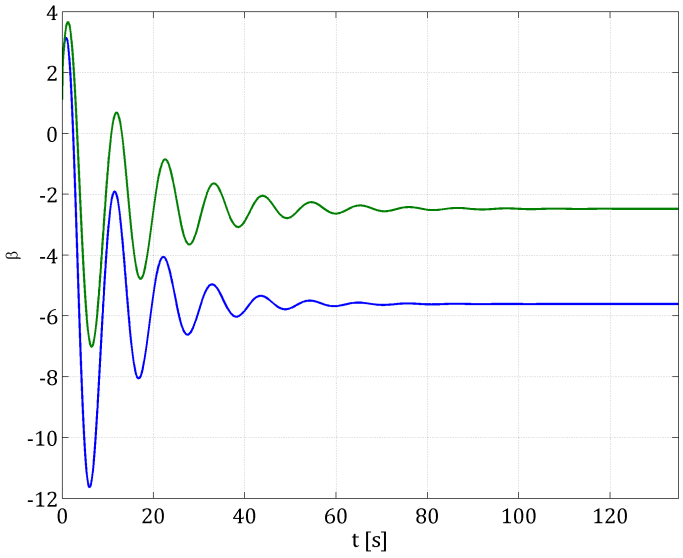

Figure 4.16: History of the orientation of the drone with respect to the ground (β) for cases 1 (—) and 2 (—)

The decrease in γ allows the drone to pitch to an angle that is closer to the horizontal.

4.5.2 Flapping wings & aerodynamic option 2

The cases drawn to comparison in this section are:

- Fixed wing configuration with variable drag and $\alpha_{t_I} = -2.58°$ (—)
- Flapping wing configuration with variable drag, $\alpha_{t_I} = -2.58°$ and a heaving amplitude $h_0 = 0.02c$ (—)
- Flapping wing configuration with variable drag, $\alpha_{t_I} = -2.58°$ and a heaving amplitude $h_0 = 0.5c$ (—)

It can be seen that the behaviour of the body with a flapping wing of this section follows the same behaviour as the one of section 4.4.2. The main difference between fixed and flapping wings can be appreciated at the beginning of the temporal response. As the perturbations die out and the equilibrium position is reached, the values of the forces will oscillate due to the periodic change in the angle of attack, as can be seen in figures 4.17 and 4.18. The X^I force oscillates around zero as it could only be expected.

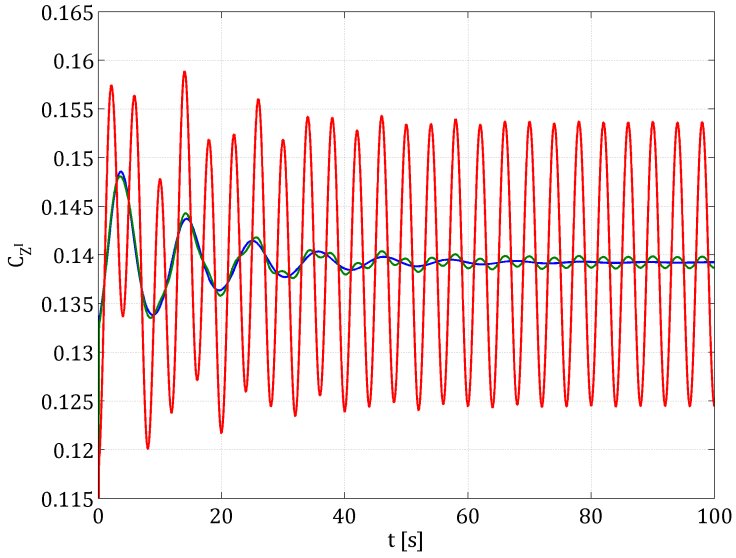

Figure 4.17: Z^I force coefficient for cases 1 (—), 2 (—) and 3 (—)

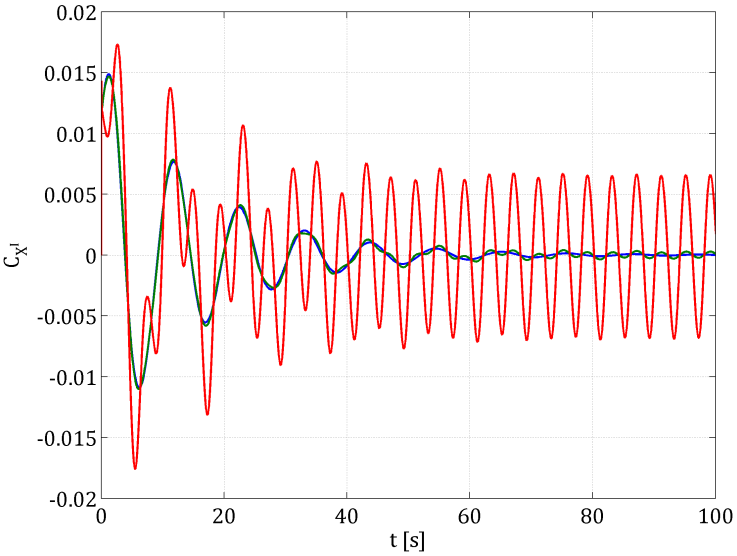

Figure 4.18: X^I force coefficient for cases 1 (—), 2 (—) and 3 (—)

Due to the oscillation in the lift coefficient, the speed at which the aircraft must move is also changing periodically as seen in figure 4.20.

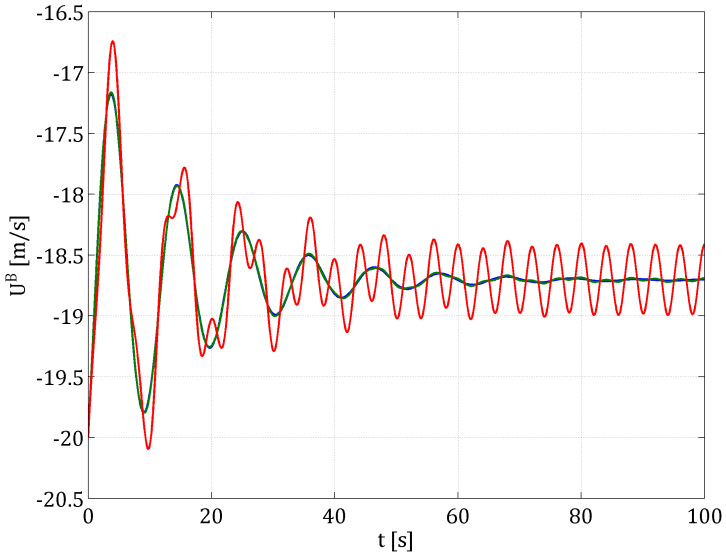

Figure 4.19: Forward velocity in body axes for cases 1 (—), 2 (—) and 3 (—)

In figures 4.20 and 4.21, the mean results of the flapping are the same as the ones of the fixed wing. This is probably an area of improvement of the code as with flapping wings thrust can be generated.

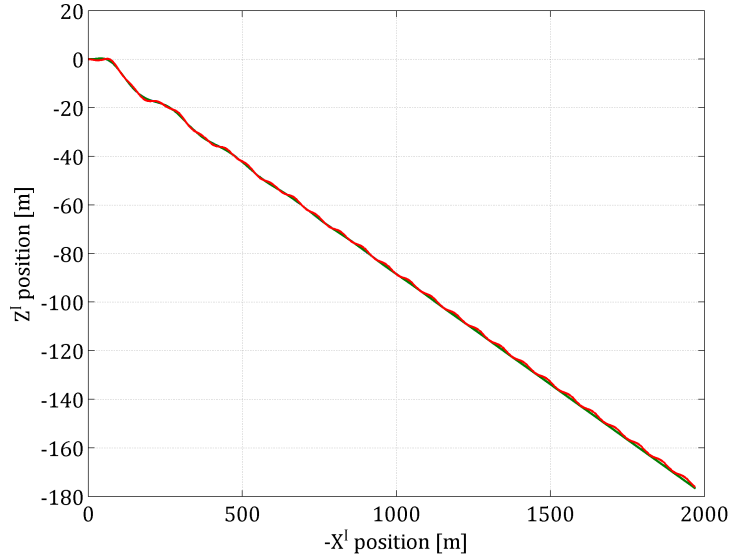

Figure 4.20: Trajectory followed by the glider for cases 1 (—), 2 (—) and 3 (—)

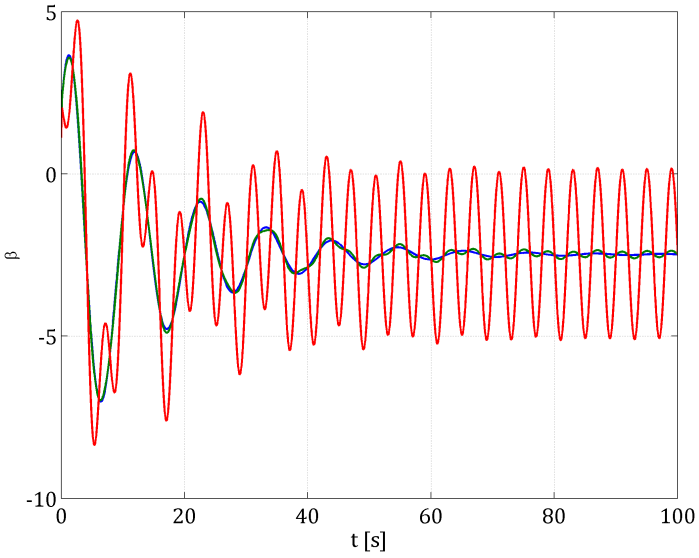

Figure 4.21: History of the orientation of the drone with respect to the ground (β) for cases 1 (—), 2 (—) and 3 (—)

4.6 Computational considerations

The cases run in this chapter had had a time step size of $\Delta t = 0.00065s$, that is the time step size that the aerodynamic code of *option 2* needed in order to make accurate computations of the forces. Of course, the smaller the time step, the more computational time is demanded. One possibility to reduce the computational time could be to decrease the initial velocity at which the drone is flying (see equation 2.31) as to decrease the Δt. Another possibility would be to decrease the number of panels of the wing and/or the wake. As always, this is a trade off between the accuracy and the time needed to compute the results.

With the configuration used in this project, a simulation run for 200 seconds with *option 2* takes approximately three days to be resolved, with no mayor change from one cases with fixed or flapping wings or with the computation of the drag. However, implementing the aerodynamic forces with *option 1* the simulation spends 1.5 - 2 hours in total. Surely all the nonlinear effect coming from the unsteadiness of the problem are not accounted for.

CHAPTER

FIVE

Conclusions

5.1 Summary

In this project, the dynamic modeling of a MAV has been generated. In order to do so, several methods that needed to be applied have been selected. The equations of motion coming from Newton's Second Law are the bases of the dynamic analysis. An Adam Bashforth second order method has been the responsible of the integration of the variables. The rotation of the body with respect an inertial reference frame has been computed by means of quaternions. This allows the code to avoid singularities that can be found in other methods such as the Euler angles.

A fundamental decision that has been made is the method used to compute the aerodynamic forces. This is a crucial part as the only two kind of forces applied to the MAV in this study are the aerodynamic forces and the weight. Two methods have been applied and integrated with the dynamic calculations so the computation of the motion and of the forces applied to the body has been solved together, they are linked and dependent on each other. The two aerodynamic methods used have been: first a linearized estimation of the forces using stability derivatives while the second one was an unsteady panel method to assess the lift and pitching moment of the wing. The parasite drag of the body has been imposed whereas the induced drag has been computed for some case and imposed in others.

The results have been performed for fixed and flapping wings, and for all cases equilibrium of forces and stable flight have been achieved. For fixed wings it has been seen that the linearized method expected a higher aerodynamic efficiency than the one found by the panel method. The implies a steeper descend for the second option. The angle of attack needed for *option 1* has been appreciated to be smaller than the one needed for *option 2*.

The results with induced drag computed by the aerodynamic code of *option 2* are not reliable enough and a better understanding and estimation techniques are needed. This final part is still in progress.

5.2 Future research

The first of the remaining tasks that could be done is to apply an aerodynamic method with two separated wings instead of a single wing. This would allow a more realistic study of the flight of a FWMAV. In addition to that, it would also lead to the possibility of analyzing the lateral behaviour of the body as antisymmetric flight will be able to be performed.

Another task that could be implemented is the refinement of the MAV model created in XFLR5 as to add a fuselage to the design. The stability analysis could be further improved by distributing in a different manner the mass along the drone that could direct towards a more efficient design.

Apart from the allocation of the mass in the body, mass could also be located in the wings so that the moments of inertia will change as the wings move. This would imply more representative cases even if the mass of the wings in principle is a small component of the total mass of the system.

Finally, the motion of the MAV could be further improved by means of a control system arrangement so that the vehicle could fly at different conditions which is essentially one of the goals of the design of any MAV.

APPENDIX

A

Aircraft data of Lockheed Jetstar

A.1 Flight conditions and aircraft characteristics

The aircraft is flying at sea level conditions at $M = 0.4$ with a free stream velocity of $u_{TAS} = 265\ kts = 136.33\ m/s$. The mass of the aircraft is equal to $m = 38205\ lbs = 17329\ kg$. The geometric characteristics of this aircraft are the following:

Span	b = 16.38 m	Mean chord	c = 3.33 m
Surface	S = 50.40 m^2	Distance from tail to CG	l_t = 7.37 m

Table A.1: Characteristics of the Lockheed JetStar

The moments of inertial expressed in body axis are:

$$I_x = 161064\ kg \cdot m^2 \qquad I_{xz} = 6863\ kg \cdot m^2$$
$$I_y = 182479\ kg \cdot m^2 \qquad I_{xy} = I_{yz} = 0\ kg \cdot m^2$$
$$I_z = 330210\ kg \cdot m^2$$

Table A.2: Moments of inertia of the Lockheed JetStar

A.2 Stability derivatives

The stability derivatives are computed with information from the drag, lift and moment coefficients from [16] and following the equations explained there to compute the stability derivative coefficients. The way to transform from non-dimensional to dimensional magnitudes can be found in [15].

Longitudinal derivatives			
Non-dimensional		Dimensional	
C_{x_u}	-0.0500	X_u	-210.4213 kg/s
C_{x_w}	0.0900	X_w	378.7584 kg/s
C_{x_q}	0	X_q	0 $kg \cdot m/s$
$C_{x_{\dot{\alpha}}}$	0	$X_{\dot{\alpha}}$	0 $kg \cdot m/s$
C_{z_u}	0	Z_u	-2494 kg/s
C_{z_w}	-5.2	Z_w	-2188.4 kg/s
C_{z_q}	-0.3709	Z_q	-2599.8 $kg \cdot m/s$
$C_{z_{\dot{\alpha}}}$	-0.1266	$Z_{\dot{\alpha}}$	-6.5118 $kg \cdot m/s$
C_{m_u}	-0.0280	M_u	-392.56 kgm/s
C_{m_w}	-0.6000	M_w	-8421.1 kgm/s
C_{m_q}	-0.8200	M_q	-19150 $kg \cdot m^2/s$
$C_{m_{\dot{\alpha}}}$	-0.2800	$M_{\dot{\alpha}}$	-47.9661 $kg \cdot m^2/s$

Table A.3: Longitudinal derivatives of the Lockheed JetStar

Lateral derivatives			
Non-dimensional		Dimensional	
C_{y_v}	-0.7000	Y_v	-2945.9 kg/s
C_{y_p}	0.1779	Y_p	1022.3 $kg \cdot m/s$
C_{y_r}	0.3559	Y_r	2044.6 $kg \cdot m/s$
C_{l_v}	-0.0800	L_v	-5515.7 $kg \cdot m/s$
C_{l_p}	-0.3660	L_p	-413420 $kg \cdot m^2/s$
C_{l_r}	0.0600	L_r	67773 kg $\cdot m^2/s$
C_{n_v}	0.1200	N_v	8273.6 $kg \cdot m/s$
C_{n_p}	-0.0800	N_p	-90364 $kg \cdot m^2/s$
C_{n_r}	-0.1600	N_r	-180730 $kg \cdot m^2/s$

Table A.4: Lateral derivatives of the Lockheed JetStar

APPENDIX

B

Graphs of the natural modes of an aircraft

B.1 Longitudinal modes

In addition to the phugoid mode, the short period mode has been studied. This motion is a high frequency and high damping performance. For this reason, the time taken for this oscillatory motion to die out is short ($\sim 10s$), significantly smaller than for the phugoid mode ($\sim 1000s$). This can be appreciated in figures B.1 and B.2.

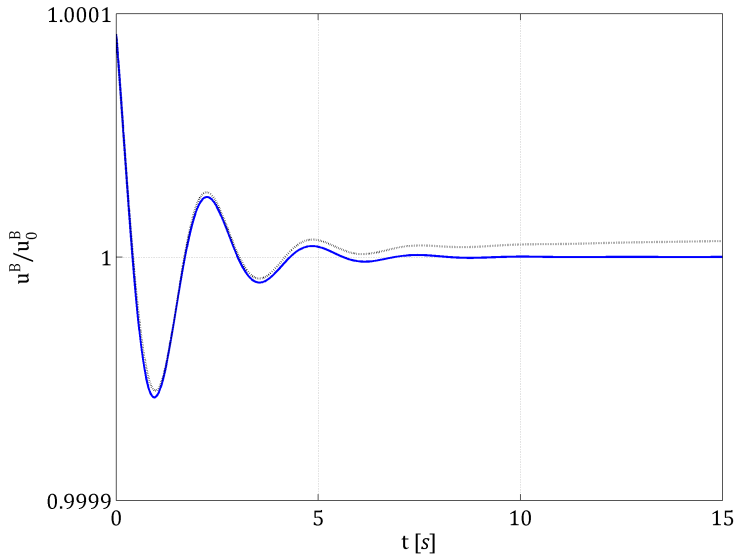

Figure B.1: Short period X velocity (u) result for the Matlab linear approach and *DyMoFlaps*

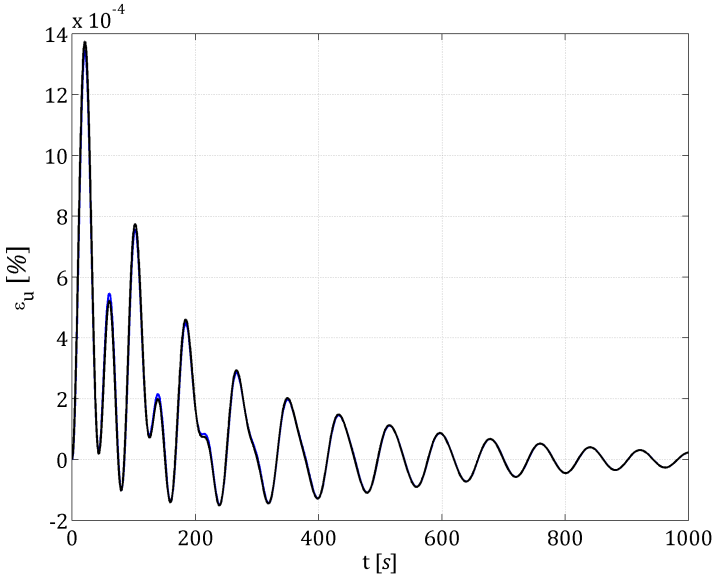

Figure B.2: Short period error in u between the two codes for different time step sizes, $\Delta t = 0.001\ s$ (—) and $\Delta t = 0.0001\ s$ (—)

B.2 Lateral modes

The two modes that are presented in this section are the spiral mode and the rolling convergence. Both are non oscillatory natural modes of the aircraft.

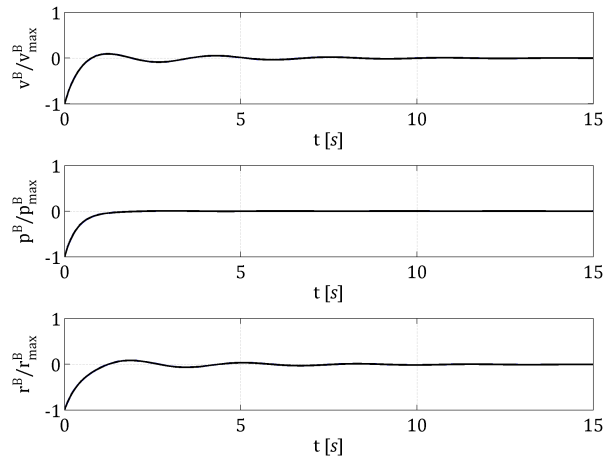

Figure B.3: Rolling convergence history of the lateral velocity and the roll and yaw rates for the Matlab integration (—) and *DyMoFlaps* (—)

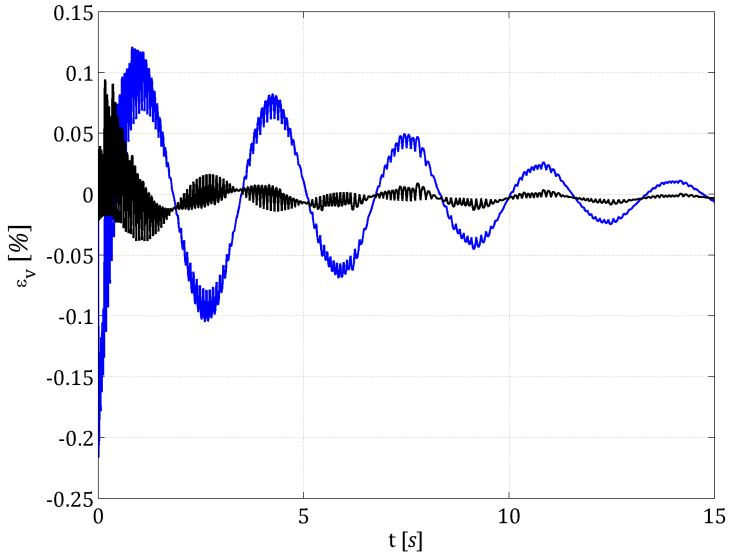

Figure B.4: Rolling convergence error between the lateral velocity solutions for $\Delta t = 0.001\ s$ (—) and $\Delta t = 0.0001\ s$ (—)

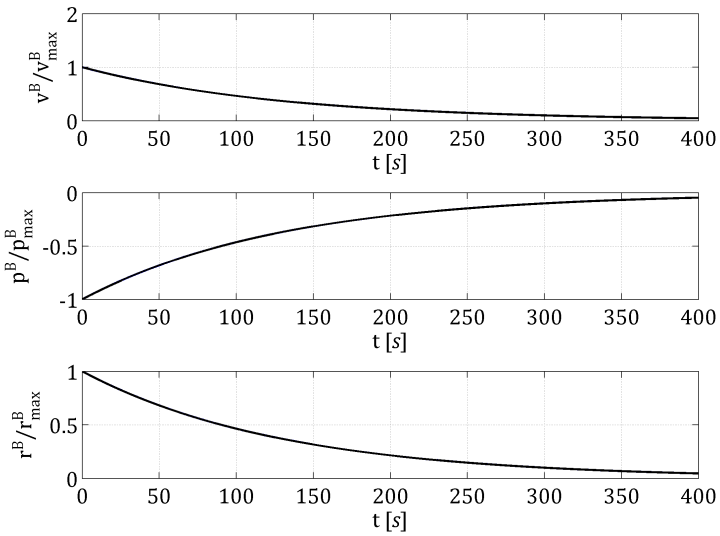

Figure B.5: Spiral mode history of the lateral velocity and the roll and yaw rates for the Matlab integration (—) and *DyMoFlaps* (—)

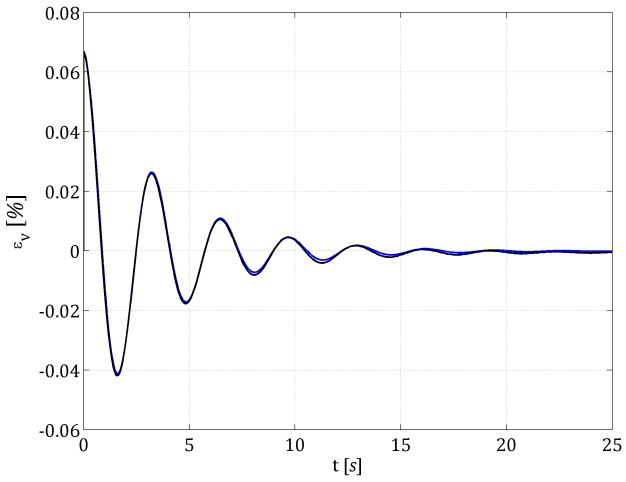

Figure B.6: Error between the lateral velocity solutions for $\Delta t = 0.001\ s$ (—) and $\Delta t = 0.0001\ s$ (—)

APPENDIX

C

Aircraft data of drone generated in XFLR5

C.1 Flight conditions and aircraft characteristics

The aircraft is flying at sea level conditions with a free stream velocity of $u_{TAS} = 20m/s$. The moments of inertial expressed in body axis are:

$I_x = 0.773\ kg \cdot m^2$ $\quad$ I_{xz} = -6.477 10^{-6}kg $\cdot m^2$
$I_y = 0.09003\ kg \cdot m^2$ $\quad$ $I_{xy} = I_{yz} = 0\ kg \cdot m^2$
$I_z = 0.8631\ kg \cdot m^2$

Table C.1: Moments of inertia of the drone

C.2 Stability derivatives

These stability derivatives are taken directly from XFLR5. The reference conditions taken into account to compute these derivatives are steady level flight where $Lift = Weigth$ and zero moment state ($\mathbf{M} = \mathbf{0}$). The way to transform from non-dimensional to dimensional magnitudes can be found in [15].

Lateral derivatives			
Non-dimensional		Dimensional	
C_{y_v}	-0.7000	Y_v	-2945.9 kg/s
C_{y_p}	0.1779	Y_p	1022.3 $kg \cdot m/s$
C_{y_r}	0.3559	Y_r	2044.6 $kg \cdot m/s$
C_{l_v}	-0.0800	L_v	-5515.7 $kg \cdot m/s$
C_{l_p}	-0.3660	L_p	-413420 $kg \cdot m^2/s$
C_{l_r}	0.0600	L_r	67773 $kg \cdot m^2/s$
C_{n_v}	0.1200	N_v	8273.6 $kg \cdot m/s$
C_{n_p}	-0.0800	N_p	-90364 $kg \cdot m^2/s$
C_{n_r}	-0.1600	N_r	-180730 $kg \cdot m^2/s$

Table C.2: Lateral derivatives of the drone

Longitudinal derivatives			
Non-dimensional		Dimensional	
C_{x_u}	-4.5 $\cdot 10^{-4}$	X_u	-0.0516 kg/s
C_{x_w}	0.0826	X_w	0.6639 kg/s
C_{x_q}	0	X_q	0 $kg \cdot m/s$
$C_{x_{\dot{\alpha}}}$	0	$X_{\dot{\alpha}}$	0 $kg \cdot m/s$
C_{z_u}	-4.8 $\cdot 10^{-5}$	Z_u	1.9610 kg/s
C_{z_w}	-5.7416	Z_w	46.1395 kg/s
C_{z_q}	10.706	Z_q	8.6033 $kg \cdot m/s$
$C_{x_{\dot{\alpha}}}$	0	$Z_{\dot{\alpha}}$	0 $kg \cdot m/s$
C_{m_u}	-7.9 $\cdot 10^{-7}$	M_u	-1.3 $\cdot 10^{-6}$ $kg \cdot m/s$
C_{m_w}	-2.2282	M_w	-3.5912 $kg \cdot m/s$
C_{m_q}	-27.536	M_q	-22.1279 $kg \cdot m^2/s$
$C_{x_{\dot{\alpha}}}$	0	$M_{\dot{\alpha}}$	0 $kg \cdot m^2/s$

Table C.3: Longitudinal derivatives of the drone

C.3 Mass distribution

The mass around the drone is placed part in the wing and in the tail and the rest is distributed as point masses along the structure. The wing was a homogeneously distributed mass of 0.8 kg and the tail has a mass of 0.2 kg. The point masses are distributed as seen in table C.4. Keep in mind that the reference frame that is used to stay the location of the masses is the one used by XFLR5 and is the one shown in figure 2.5.

Mass $[kg]$	x $[m]$	y $[m]$	z $[m]$
0.74	-0.15	0	0
0.2	0.31	0	0
0.08	0.1	0.2	0
0.08	0.1	-0.2	0
0.03	0.1	0.9	0
0.03	0.1	-0.9	0
0.02	0.05	0	0

Table C.4: Point masses of the drone

APPENDIX

D

Project budget

The project budget is estimated in this section. The main items are detailed below.

- **Computational time.** This refers to the HPC cluster which has been used for the computations. An estimation based on the Spanish CESGA center [21] has been made, and the hour of computing has been priced to €0.2 per hour and processor. It has been estimated than approximately 700 hours of computation have been needed, at a mean of 2 processors. This adds up to a total of €300.

- **MATLAB license.** Matlab has been used for computations and post-processing. A license for academic purposes is priced at €500.

- **Base computer.** In order to make use of the software and to be able to do the present project, a computer has been needed. It has been an Intel-i7, Toshiba computer, with Microsoft Windows installed on it. Its price is €750.

- **Hours of work.** The price per work hour has been estimated with the price of an engineer with low experience for a research project. It has been estimated at €25 per hour of work. Around 400 hours of work have been needed for the present project, leading to a price of €10,000.

Therefore, the total cost of the project is shown in the following table.

Item	Price (€)
HPC time	300
MATLAB license	500
Computer	750
Work hours	10,000
Total cost	**11,550**

Table D.1: Cost analysis of this project

Bibliography

[1] Conver, Tim, "Nano Hummingbird", *www.avinc.com/nano*, (2015)

[2] Shyy, Wei and Aono, Hikaru and Kang, Chang-kwon and Liu, Hao, "An introduction to flapping wing aerodynamics", Cambridge University Press, (2013).

[3] Shyy, Wei and Aono, Hikaru and Chimakurthi, Satish K. and Trizila, Pat and Kang, Chang-kwon and Cesnik, Carlos E. and Liu, Hao, "Recent progress in flapping wing aerodynamics and aeroelasticity", Progress in Aerospace Sciences, Vol 46, Pgs 284-327, (2010).

[4] Orlowski, Christopher T. and Girard, Anouck R., "Dynamics, stability, and control analyses of flapping wing micro-air vehicles", Elsevier, Progress in Aerospace Sciences, Vol 51, Pgs 18-30, (2012).

[5] Alexander, David E., "Nature's flyers; birds, insects, and the biomechanics of flight", The Johns Hopkins University Press, (2002).

[6] Sane, Sanjay P., "The aerodynamics of insect flight", Journal of Experimental Biology, Vol 206, (2003).

[7] Uhlmann, Markus, "An inmersed boundary method with direct forcing for the simulation of particulate flows", Journal of Computational Physics, Vol 209, Pgs 448-476, (2005).

[8] Grauer, Jared A. and Hubbard Jr, James E., "A Multibody Model of an Ornithopter", Journal of Guidance, Control, and Dynamics, AIAA, (2009).

[9] Suzuki, Kosuke and Minami, Keisuke and Inamuro, Takaji, "Lift and thrust generation by a butterfly-like flapping wing-body model: immersed boundary-lattice Boltzmann simulations", Journal of Fluid Mechanics, Vol 767, Cambridge University Press (2015).

[10] Caetano, J. V . and Weehuizen, M. B. and de Visser, C. C. and de Croon, G. C. H. E. and Mulder, M., "Rigid-Body Kinematics Versus Flapping Kinematics of a Flapping Wing Micro Air Vehicle", Journal of Guidance, Control, and Dynamics, AIAA, (2015).

[11] Ma, K. and Chirarattananon, P. and Fuller, S. and Wood, R., "Controlled flight of a biologically inspired, insect-scale robot", Science, Vol 340, Pgs 603–607, (2013).

[12] Craig, Whitlock, "Near-collisions between drones, airliners surge, new FAA reports show", The Washington Post, (2015)

[13] Federal Aviation Administration, "Unmanned Aircraft Systems (UAS) Regulations Policies", *www.faa.gov/uas/regulations$_p$olicies*, (2015)

[14] Tewari, Ashish, "Atmospheric and Space Flight Dynamics: Modeling and Simulation with MATLAB® and Simulink®". Modeling and Simulation in Science, Engineering and Technology. Birkhäuser (2007).

[15] Etkin, Bernard and Reid, Lloyd D., "Dynamics of Flight: Stability Control", John Wiley and Sons, 3rd Edition, (1996).

[16] Heffley, Robert K. and Jewell, Wayne F., "Aircraft Handling Quality Data", NASA CR-2144, Dec, (1972).

[17] Deperrois, Andre, " XFLR5 Official Web Page", *www.xflr5.com*, (2015)

[18] Deperrois, Andre, "Modal analysis and experimental validation", *www.xflr5.com/docs/XFLR5$_M$ode$_M$easurements.pdf*, *February*(2011)

[19] Arranz, Gonzalo, "Analysis of flapping wings. Development of an unsteady potential model for a flapping wing drone ", (Bachelor Thesis in progress), October (2015)

[20] Katz, Joseph and Plotkin, Allen, "Low speed aerodynamics", Cambridge University Press, Vol 13, (2001)

[21] CESGA company web page, *www.cesga.es*